Heliyon 6 (2020) e05554

Contents lists available at ScienceDirect

Heliyon

journal homepage: www.cell.com/heliyon

Review article

Methods and variables in Electrical discharge machining of titanium alloy – A review

A. Pramanik [a,*], A.K. Basak [b], G. Littlefair [c], S. Debnath [d], C. Prakash [e], Meinam Annebushan Singh [f], Deepak Marla [f], Ramesh Kumar Singh [f]

[a] School of Civil and Mechanical Engineering, Curtin University, Bentley, WA, Australia
[b] Adelaide Microscopy, The University of Adelaide, Adelaide, SA, Australia
[c] Faculty of Design and Creative Technologies, Auckland University of Technology, New Zealand
[d] Department Mechanical Engineering, Curtin University Sarawak, Sarawak, Malaysia
[e] School of Mechanical Engineering, Lovely Professional University, Phagwara, Punjab, India
[f] Department of Mechanical Engineering, Indian Institute of Technology Bombay, India

ARTICLE INFO

Keywords:
Materials science
Mechanical engineering
Metallurgical engineering
Manufacturing engineering
Metals
Machining
Structural behavior
Titanium alloy
Electrical discharge machining
Surface integrity
Material removal rate

ABSTRACT

Titanium alloys are difficult to machine using conventional methods, therefore, nonconventional processes are often chosen in many applications. Electrical discharge machining (EDM) is one of those nonconventional processes that is used frequently for shaping titanium alloys with their respective pros and cons. However, a good understanding of this process is very difficult to achieve as research results are not properly connected and presented. Therefore, this study investigates different types of EDM processes such as, wire EDM, die-sink EDM, EDM drill and hybrid EDM used to machine titanium alloys. Machining mechanism, tool electrode, dielectric, materials removal rate (MRR), and surface integrity of all these processes are critically analysed and correlated based on the evidence accessible in literature. Machining process suffer from lower material removal rate and high tool wear while applied on titanium alloys. Formation of recast layer, heat affected zone and tool wear is common in all types of EDM processes. Additional challenge in wire EDM of titanium alloys is wire breakage under severe machining conditions. The formation of TiC and TiO_2 are noticed in recast layer depending on the type of dielectrics. Removal of debris from small holes during EDM drilling is a challenge. All these restricts the applications EDMed titanium alloys in high-tech applications such as, aerospace and biomedical areas. Most of these challenges come up due to extraordinary properties such as, low thermal conductivity, high melting point and high hardness, of titanium alloys. Though hybrid EDM has been introduced and there is some work on simulation of EDM process, further developments in EDM of this alloy is required for widening the application of this methods.

1. Introduction

Conventional or traditional machining methods remove materials by plastic shearing for example, formation of chip (for example, broaching, drilling, milling, turning), abrasion (for example, lapping, grinding) or micro-chipping (for example, polishing micro-abrasive and blasting). However, it is costly to use traditional machining processes to difficult-to-machine materials for example, nickel-based alloys and titanium-based alloys in general (Pramanik, 2014a; Pramanik and Littlefair, 2014; Pramanik et al., 2009). This is due to high tool wear, extended machining time and, impossible to achieve some complex/intricate shapes by this process. Mechanical properties and metallurgical distinctiveness of titanium alloys make it complicated and costlier to machine than that of steels with similar range of hardness (Pramanik, 2014b; Pramanik and Littlefair, 2015). Despite poor machinability, titanium/titanium alloys are widely used in medical (for example, dental implants, spinal fusion cages, finger and toe replacements and bone plate expandable ribs cages), aerospace, marine, chemical processing and automobile sectors (Pandey and Dubey, 2012).

Hence, non-traditional machining methods are applied to process titanium alloys. Amongst different non-traditional machining procedure, EDM is widespread owing to its adaptable ability to cut difficult-to-

* Corresponding author.
E-mail address: alokesh.pramanik@curtin.edu.au (A. Pramanik).

https://doi.org/10.1016/j.heliyon.2020.e05554
Received 21 May 2020; Received in revised form 2 July 2020; Accepted 16 November 2020

machine materials in complex shapes (Pramanik et al., 2018; Pramanik and Basak, 2016). During EDM, the workpiece is dipped in dielectric liquid to create a encouraging surrounding for electric sparks to happen (Pramanik et al., 2018; Pramanik et al., 2018; Pramanik and Littlefair, 2016). Spark erosion takes place in the vicinity of electrodes and forms expected three/two dimensional figures by melting/evaporating the workpiece material (Kumar et al., 2018; Pilligrin et al., 2018; Pramanik et al., 2019). It is a promising technique for various materials irrespective of its toughness and hardness, as long as those are conductive electrically (Pramanik, 2014a; Pramanik et al., 2018). In this process, an electrode acts as a tool and the workpiece material itself act as other electrode. The dielectric liquid acts as heat absorber and carries heat and debris away from the machining zone (Alshemary et al., 2018; Pramanik, 2014a). The higher melting temperature, specific heat and electric resistivity of titanium alloys necessitate added energy to vaporize or melt this material (Mahardika et al., 2008) during EDM process. In addition, poor thermal expansion coefficient and thermal conductivity of titanium alloy makes the process more challenging in terms of heat transfer and cause localized discharges, arcing, short-circuiting and tool failure. These scenarios decrease the efficiency of the process, results in lower material removal rate (MRR) or even damaged machined surfaces (Gu et al., 2012). Additionally, collision or adhesion of the molten drops on machined surface is very evident and results in mushy platelets formation as well as thicker recast layer (Soni, 1994).

The above information indicates that there are numerous studies on different EDM processes of various titanium alloys and promising results are obtained so far. All the studies are not linked and organised scientifically to have a clear understanding of the processes when used for titanium alloys. Therefore, it is imperatively needed to investigate material removal mechanism, tool electrode, dielectric, materials removal rate (MRR), and surface integrity for scientifically correlate the available information. The understandings and outcomes from this investigation will be beneficial to professional and researchers in this field to extend the applications and processing of these alloys more economically. The research methodology of this investigation is given in Figure 1.

2. Wire-electrical discharge machining (WEDM)

In this procedure, a metallic wire acts as tool electrode in EDM procedure that is comparable to outline cutting using a band saw. The wire electrode moves through computer assisted numerical control to attain three dimensional forms (Kumar, Khan and Muralidharan, 2019; Mukherjee and Chakraborty, 2012).

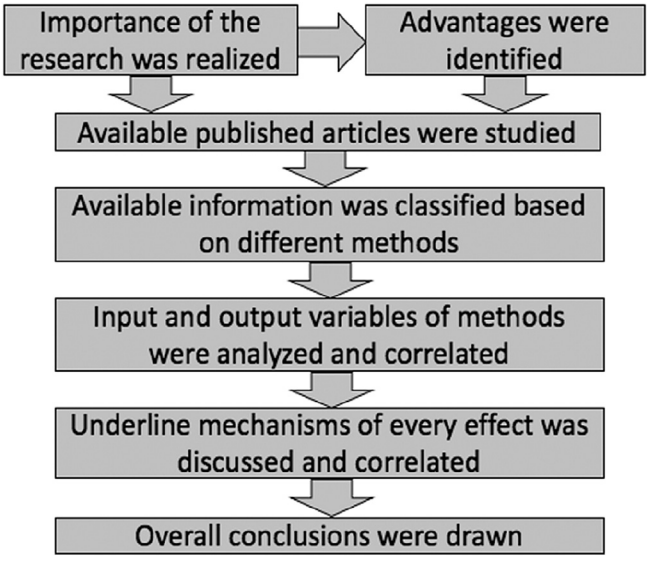

Figure 1. Flowchart of this research.

2.1. Mechanism

Generally, the nature of titanium alloy WEDM is identical to that of other metal alloys. The temperature of individual spark is estimated as 20000 °C which erodes away a small (10^{-6} – 10^{-4} mm^3/spark) amount of material through melting and evaporating. Part of that material is removed from the machining region by the dielectric liquid (Pramanik, 2014a) where the workpiece is submerged. The wire electrode is kept under a constant predefined tension to minimize the lateral vibration of the wire, and thus circumvent the tendency of incurring dimensional inaccuracy in machined workpiece (Mukherjee et al., 2012). In this case, wire electrode experience two relative motions with respect to workpiece. Those are (a) the wire speed which it the wire electrode travel rate from the top spool to the bottom spool and (b) wire feed which is the wire electrode's rate of moving towards the workpiece while machining. As titanium alloys require higher temperature during WEDM, wire electrode also starts to degrade as soon as machining commences. Therefore, a cleaner machining at the top of the workpiece and, comparatively dirtier machining processes coupled with degraded wire electrode are usually noticed at the bottom of the workpiece (Pramanik & Basak, 2016, 2018). The degree of dirtiness and degradation of wire electrode is highly influenced by the thickness of workpiece and the associated machining parameters.

Typical WEDM process for titanium alloy is shown in Figure 2 (a) where the wire degrades severely as it travels through the machining zone. In addition, the amount of debris increases towards the bottom. In certain situations, especially for titanium alloys, the wear rate of wire material very high while removing workpiece material, which reduces the diameter of wire. This condition leads to wire rupture at the position of smallest cross-section area under the influence of the maintained wire tension (Pramanik and Basak, 2018).

Higher temperature is required to melt them down titanium alloy during removal process. Heat generated (Q) in machining zone, as shown in Figure 1b is partly used in melting and vaporizing the workpiece material. A part of it (Q_2) is conducted in titanium alloy and the rest (Q_1) is absorbed by the dielectric. The amount of heat conducted in titanium is very small due to its lower thermal conductivity. Therefore, temperature (T_1) in machined surface is considerably greater than that (T_2) below the machined surface. This causes intense heat concentration in thin layer of machined surface and a significant temperature gradient is experienced by machined surface along the depth of the workpiece. The top layer of machined surface also goes through quenching process due to continuous circulation of dielectric. Therefore, properties of machined surface changes significantly compare to that of bulk material. The recast layers and heat-affected zone are thus prominent on machined titanium alloy surface due to high temperature on surface and significant temperature gradient towards the bulk material.

2.2. Wire electrode

Lower melting temperature of tool electrode material induces higher wear. Generally, diameters of wires are 0.2 and 0.3 mm for finish and rough, respectively. Nevertheless, typically the wire diameter differs from 0.05 to 0.3 mm (Mukherjee et al., 2012). These are usually made from tungsten, copper, brass, zinc-coated brass and molybdenum as well as multicoated wires. Copper-tungsten or copper, brass and graphite wires are commonly utilized to WEDM of titanium alloy. Brass material is relatively more popular due to its higher strength, higher electric conductivity, better draw-ability and aptitude to attain high tolerance specifications (Antar et al., 2010). However, brass wire coated with zinc performs better on titanium alloys due to its relatively higher melting temperature and strength than that of brass wire (Nourbakhsh, 2012). Moreover, the effectiveness of machining process is enhanced by zinc coating as the coating induces cooling effect to protect the core. The addition of zinc coating on brass also reduces the melting point of wire as well as improves spark generation and reduces time for dielectric

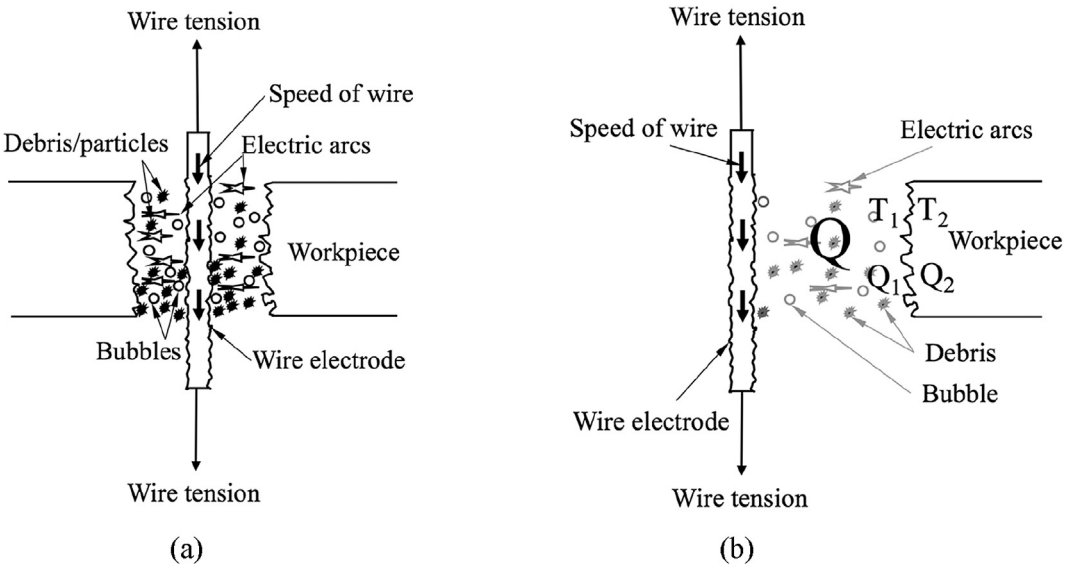

Figure 2. Typical WEDM process for titanium alloy: (a) mechanical and electrical processes, and (b) thermal processes.

ionization, which results in increased feed rate. The machining feed for high-speed brass wire is around 1.5 folds lesser than that of zinc-coated wire in similar machining conditions (Nourbakhsh, 2012). Figure 3 presents surfaces of titanium alloy machined with zinc-coated and high-speed brass wires under same conditions. As noted from the pictures, uncoated wire generated surface with more melted cracks, craters, globules of debris and drops compare to that of coated wire because of greater thermal conductivity and lower melting temperature of zinc coated wire as mentioned above (Nourbakhsh, 2012).

Wire breakage during EDM of titanium alloy is very frequent and the contributing factors are thermal load, tension in wire and dielectric flushing capabilities (Nourbakhsh, 2012). Wire failure frequency is directly and inversely proportionated to pulse on-time and pulse off-time, correspondingly. Greater discharge energy produces excessive heat to cause wire failure. The excessive heat softens wire material and stress built up while the procedure drives beyond the ultimate strength of wire material. The occurrences of wire break are greater at upper wire tension and lesser flushing pressure. Wire rupture strikes at sudden excessive temperature because of formation of undesirable arcs whilst the debris/wastes of EDM are not cleaned appropriately. Larger tension in wire might rupture the wire at lesser temperature as well in machining region. Wire rupture could be instantaneous and/or gradual, nevertheless, the ruptured wire tips undergo necking (Pramanik and Basak, 2018). The frequency of wire failure increases while machining complex forms due to rapid change of discharge energy alongside the thickness of workpiece. Moreover, the dielectric flushing capability also affects the wire failure, which gets more pronounced during machining for thicker workpieces. Relatively higher wire speed and feed rate reduce machining load of the wire to a relatively shorter time thereby lowering the erosion rate and rupture rate (Nourbakhsh, 2012).

2.3. Dielectric fluid

According to literature, only de-ionized or distilled water have been used so far for wire-EDM of titanium alloys (Antar et al., 2010; Nourbakhsh, 2012; Prohaszka et al., 1997; Yan and Lai, 2007). These dielectric fluids are also used during wire-EDM of other materials (Pramanik et al., 2018; Pramanik et al., 2015; Pramanik and Littlefair, 2016) due to its low viscosity, rapid cooling effect as compared to that of hydrocarbon oil. Moreover, the lower cost and environmental friendly

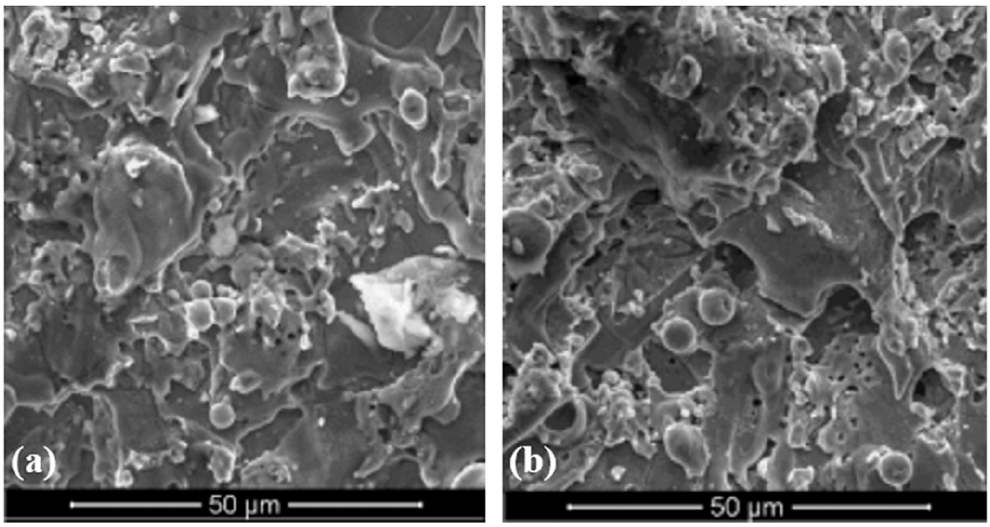

Figure 3. SEM micrographs of titanium alloy machined with (a) zinc-coated brass and (b) high-speed brass wires (Nourbakhsh et al., 2013).

behavior further aids towards the application of deionized/distilled water as a promising dielectric for machining various materials (Alias et al., 2012; Rao et al., 2010).

2.4. Material removal rate (MMR)

Nourbakhsh, 2012 suggested that dielectric injection pressure, machining voltage, wire tension, wire speed and servo reference voltage are not substantial process variables for feed rate that affect MRR. According to (Ghodsiyeh et al., 2012), the significant parameter is peak current which influences MRR. (Devarajaiah and Muthumari (2018) investigated the effect of interactions for different combinations of pulse-on-time, pulse-off-time, current and wire speed on the material removal rate. It was noted that the increase of wire speed and current increases the MRR but the pulse-off time does not influence it significantly. Initially the MRR increases with the increase of pulse-on time then decreases with the further increase of pulse-on time. The peak current upsurges local temperature and discharge energy, which significantly increases the MRR. Amplified spark energy increases feed rate and results in greater material removal. Generally, MRR rises with the upswing of pulse-on-time although declines as the tension in wire increases as presented in Figure 4. In addition, MRR at lesser dielectric pressure (7 MPa) is relatively lower. MRR rises and later stays nearly unchanged as the flushing pressure rises. It appears that the debris congest the machining region and sparks occur with no material removal at lower flushing pressure. Instead, a steady machining atmosphere is sustained at greater flushing pressure which results nearly constant rate of material removal (Pramanik and Basak, 2018).

2.5. Kerf width

The kerf width represents the zones over which the material was removed by the wire electrode under the action of discrete discharges, which is higher than the actual diameter of the wire (Wasif et al., 2020). Theoretically, the average kerf width can be approximated by adding wire diameter with two times the spark gap. During wire-EDM process, the kerf width is observed to be highly dependent on the discharge energy related parameters (peak current, pulse on-time and voltage) as they control the intensity of discharges and the overall spark gap as well (Alias et al., 2012). The wire material, wire tension and feed rate are other parameters which influences the net kerf width, though not as pronounced as the discharge energy related parameters. According to Sivaprakasam et al. (Sivaprakasam et al., 2014), kerf width is minimized at constant stable discharge and lower energy of discharge. Moreover, the kerf width was observed to increase with decrease in the wire tension. This is mainly due to the increased vibration of the wire electrode in the lateral direction, which in turn correlates to higher concentration of discharges in the lateral direction. Therefore, greater tension in wire contribute towards a more favorable and stable kerf width. However, a very high tension is also not desired as it increases the probability of frequent wire rupture. Lenin et al. (Lenin et al., 2014) noted that width of kerf increases as the pulse-on-time increases. In addition, taper appears near the end of machining. (Alias et al. (2012) stated that, pulse-off-time rise of 1–5 μs and peak current rise of 4–12 A upsurge the width of kerf considerably. Nonetheless, impact of pulse-off-time was greater than that of peak current. The optimal planning of machining parameters for width of kerf were 5 μs pulse-on-time, 12 A peak current, 6 N wire tension and 4 mm/min wire speed.

Width of kerfs at bottom and top of workpieces usually differ owing to wear or/and distortion of wire electrode, and alteration of dielectric properties during WEDM. The difference amongst the widths of bottom and top kerfs is minor as pulse-on-time alters. This could be because of balancing out the distortion of wire electrode with the alteration of dielectric properties because of the generation (oxide) of debris while machining (Pramanik et al., 2019). Width of kerf at the top is considerably greater than that at bottom at lesser flushing pressure which is because of impurity in dielectric at lower pressure, this alters the electrical behaviors of dielectric and reduces efficient removal of material. Furthermore, new wire electrode produces greater kerf at the top. The reduced kerf width at bottom is owing to the wire electrode wear. As the flushing pressure increases, difference amongst widths of top and bottom kerfs decrease by balancing the wear and distortion of wire electrode, and alteration of dielectric's electrical behavior. Both bottom and top widths of kerfs rise considerably as flushing pressure rises further. This is could be because of superior cooling of wire electrode that decreases distortion and wear, and cleansed spark region at greater flushing pressure (Pramanik et al., 2019).

The kerf widths at the top and bottom reduce as the wire tension increases. When the tension is lower, the wire is flexible and lengthier which increase heat input and remove additional materials; consequently, the kerf widens. On the contrary, at greater tension, wire electrode is stiffer and the wire diameter reduces which contributes to smaller width of kerf (Pramanik et al., 2019).

2.6. Surface integrity

The variation in surface topography is minimal with respect to wire feed rate. A comparatively smoother surface is obtained when MRR is lower (Alias et al., 2012). The surface quality decreases with the increase of cutting speed and almost linear with surface roughness of 2.44 μm at 2.65 mm/min machining speed. Beyond this, surface roughness deteriorates drastically with further increase of machining speed. Surface finish and dimensional errors are not affected by pulse-off-time. This fact is very significant, as for critical processing conditions, pulse-off-time could be changed according to the requirements for improved stability of the system and precision of the cut (Sarkar et al., 2005). Crater size rises with the rise of feed rate during WEDM of titanium alloys (Alias et al., 2012). A polished cross-section of rim area generated from rough wire EDM is given in Figure 5 (Klocke et al., 2011) which shows heat affected zone, recast layer and surface cracks in the machined surface. These defects could be minimized through optimizing process parameters (Antar et al., 2010; Yan and Lai, 2007).

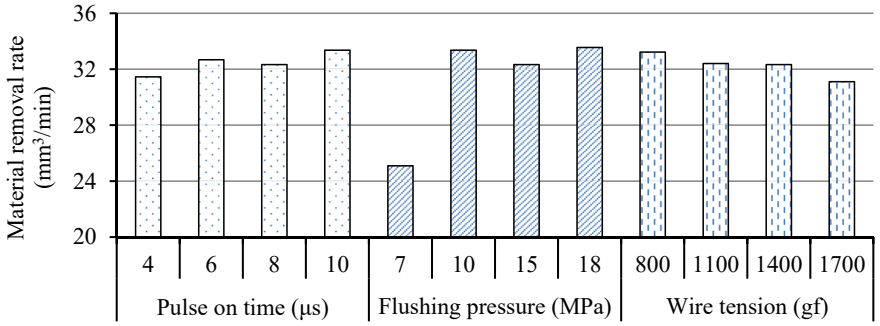

Figure 4. Influence of pulse on-time, flushing pressure and tension in wire on MRR while WEDM of titanium alloy (Pramanik and Basak, 2018).

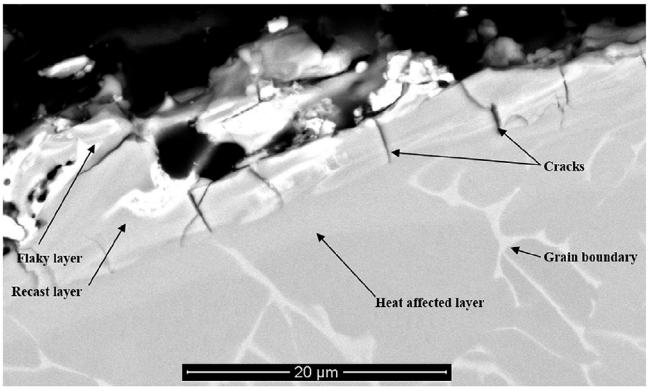

Figure 5. Cross-section of metallographic polished machined surface of Ti6Al4V after wire EDM.

Antar et al. (2010), reported WEDM of Ti6Al2Sn4Zr6Mo alloy using uncoated brass wire under depth of cut of 45 μm, voltage of 120 V, pulse-off-time of 6 μs, pulse-on-time of 0.1 μs, wire speed of 8 m/min, wire tension of 20 N and current of 0.4 A. These conditions provided surface roughness of 1.72 μm and recast layer thickness of about 9 μm. However, with several finish cut (3 cuts) by gradual change in machining parameters, average surface roughness and recast layer thickness come down to 0.48 μm and 1.5 μm, respectively, under depth of cut of 2 μm, voltage of 100 V, pulse-off-time if 0.6 μs, pulse-on-time of 0.4 μs, wire speed of 8 m/min, wire tension of 18 N and current of 0.6 A. The micro-cracks can be avoided by finish/clean cut. The residual stresses are tensile in nature on the top surface and become neutral under 80 μm from the top. The finish cut surface generates much lower residual stress (tensile) compared to that of rough-cut. Minimum damage on machined surface can be obtained after 'clean cut' which uses trapezoidal/adapted pulse shapes with a duration of 50–1000 ns under ultra-high repetition frequencies in MHz range (Antar et al., 2010).

Surface quality of titanium alloy generated from WEDM can also be improved by utilising fine-finish power supply (Aspinwall et al., 2008; Yan and Lai, 2007). This is transistor-controlled power supply, which is consists of a pulse control circuit, two snubber circuits and a full-bridge circuit to deliver the roles of anti-electrolysis, extremely little energy pulse control and high frequency. The pulse-on-time of discharge current could be reduced by tuning the capacitance in parallel to spark gap. Higher capacitance gives longer and higher resistance to limit the current, which reduce discharge current. The reduction of peak current and pulse on-time reduces recast layer thickness (Yan and Lai, 2007). (Aspinwall et al., 2008) used MOSFET field effect transistors combining with ultra-fast regaining diodes which empowered complete control on the form of electric pulse. This technique can generate trapezoidal current pulses larger than 1000 A and slope of up to 600 A/μs, which necessitates machining zone inductance of $\leq$0.5 μH. Pulses are provided with time lengths within 50–1000 ns. These ultra-short pulses in addition to the high recurrence frequencies up to 330 kHz could be additionally sliced to give ultra-high frequencies in the order of 10 MHz. In amalgamation with changed pulse forms, such as, bipolar pulses lower the surface damage notably.

The machined titanium alloy surface from DC power supply changes to blue and rusty due to oxidation through electrolysis. This degrades the quality of machined surface, enhances untimely breakage of produced components and therefore prohibit the much use of WEDMed titanium alloy in medical and aerospace fields. Though the oxidized layer may be removed by additional machining processes, those influence overall cost and accuracy of produced components. Fine-finish power supply minimizes the machined titanium alloy surface from becoming rusty and blue. Thus, fine-finish power supply requires reduced polishing time and attendant cost due to lower surface degradation (Yan and Lai, 2007).

3. Die-sinking EDM

Die-sinking EDM is different from WEDM as an anticipated die is utilized as a replacement for wire in the former case (Gu et al., 2012). The influence of different variables for example, dielectric flushing pressure, pulse-on-time, dielectric fluid, peak current, etc. on the capability of die-sinking EDM on titanium alloys are studied by various investigators (Fonda et al., 2008; Laxman and Raj, 2014).

3.1. Mechanism

Similar to WEDM, mechanism of die-sink EDM is also controlled by the properties of workpiece material. The cathodic tool polarity is disparaging in sinking EDM because of excessive tool wear, Ti6Al4V machining is not closely as lucrative as machining of various other metals (Amorim et al., 2014; Klocke et al., 2014). This is clarified by the generation of titanium carbide (TiC) in subsurface layer of the workpiece whilst the tool is anode. Carbon (C) to form TiC comes from the breakdown of hydrocarbon based dielectric fluid used during die-sink EDM. Melting temperature of TiC is double compared to Ti6Al4V and thus hard to machine by EDM. The subtraction of Ti6Al4V reaches negative values for greater discharge periods, this was due to the adhesion of material on workpieces. The removal rate of titanium alloys is generally greater than that of iron alloys when the machining starts. This is due to inferior thermal conductivity of titanium alloys, as this gives intense localized temperatures and, consequently, higher material removal (Klocke et al., 2018). Titanium carbide (TiC) does not form in the single discharge cavities. Whereas the consecutive discharges in continuous EDM reduces of anodic removal rate significantly (Fonda et al., 2008). Localized temperature increases along with the expansion of plasma channel during EDM. This decomposes and sticks carbon to electrode surfaces which un-stabilizes the system and reduces discharge efficiency as well as MRR (Chen et al., 1999). Since single discharge cavities exposed a larger diameter by an anodic tool, power concentration of every discharge is expected excessively small to detach TiC, as opposite to cathodic polarity (Klocke et al., 2018).

3.2. Tool electrode

The prime necessities of tool electrode material during die sink EDM are better electric conductivity, high melting point and lower rate of wear. Hascalik & Caydas (Hasçalık and Çaydaş, 2007) reported graphite, aluminum and copper electrode materials for die-sink of Ti6Al4V titanium alloy and found that, graphite electrode offer the uppermost MRR trailed by electrolytic copper and aluminum. However, graphite electrode also contributes towards worse surface finish and lowest wear because of its higher melting temperature under all applied conditions. Aluminum electrode displays the best performance in terms of surface roughness. Greater MRR generally comes at the expense of surface finish and afterword, inferior fatigue behaviour. A finishing cut is required in this situation to improve the performance machined parts. Sivakumar et al. (Sivakumar and Gandhinathan, 2013), utilized steel (EN24), aluminum, graphite, electrolytic copper, tungsten copper, beryllium copper, and copper impregnated graphite electrodes to machine Ti6Al4V titanium alloy. Among all these electrodes, copper impregnated graphite was found to be the best performing electrode based on MRR, electrode wear and overcut (Sivakumar and Gandhinathan, 2013). Graphite electrode can achieve a feed rate of 10.05 and 6.28 times higher than that of aluminum and copper electrodes, respectively, during die sink EDM of titanium alloy (Hasçalık and Çaydaş, 2007). Powder metallurgy copper slugs/buttons manufactured at various compressing pressures utilizing highly pure (99%) powder with the largest particle size of 50 μm have also been used (Ho et al., 2007). In this case, electrode material transported to workpiece surface was up to ~ 29 at %. However, it was ~ 78 at % for powder compact (32 MPa) electrode. Cu matrix reinforced with SiC particles composite electrode has also been used. In this case, electrode

has higher wear resistance and machined surface had a harder recast layer that was formed due to generation of new phases of TiC and $TiSi_2$ (Li et al., 2016). Mishra et al. (Mishra et al., 2018), used cryogenically conditioned copper, normal copper and tungsten material tool electrodes. Cryogenically conditioned copper electrode gave lower tool wear, better surface finish and higher MRR as compared to that of normal copper electrode. The electrode of tungsten gave rough surface and lower MRR owing to reasonably lower thermal conductivity of electrode and workpiece materials. For the same reason, presence of TiC is predominant in addition to Al_8V_5 in recast layer of workpiece material. Cryogenically conditioned copper electrode displayed comparatively more TiC precipitation than that of normal copper. The electrode might be in the shape of a solid bundled die. The bundled electrodes give increased MRR and decreased tool wear rate, and makes it reasonably more practicable while rough machining of large-area compare to that of solid electrode (Gu et al., 2012). It was found that, bundled copper hollow electrode of hexagonal shape sustained peak current of as high as 127 A which is much higher compare to what is used in solid single electrode die-sinking. Under the application of internal flushing, flow speed rises uninterruptedly from the center towards border in radial direction of tool electrode. This effective flushing covers electrode surface partly by expelled debris from melting workpiece materials and thus protects the electrodes and wear of tool takes place uniformly (Gu et al., 2012).

The consequence of EDM variables on wear of electrode is shown in Figure 6 (Hasçalık and Çaydaş, 2007) and it is evident that, wear of electrode is principally influenced by pulse off and on times. The wear of electrode also relies on electrode materials. It was noted that, electrode wear rises as pulse current and pulse-on-time rise. In addition, higher melting point of workpiece material induces lesser wear of electrode (melting point of Al = 660 °C, Cu = 1083 °C and Gr = 3300 °C) (Lee and Li, 2001). In addition, type of workpiece material is also important as formation of TiC on machined surface increases electrode wear as the melting temperature of TiC (3150 °C) is nearly double of that of Ti (1660 °C) and thus larger discharge energy is essential (Chow et al., 1999).

3.3. Dielectric fluid

The dielectric medium is usually kerosene for die sink EDM of titanium alloy (Gu et al., 2012). However, other dielectrics also serve the purpose. For example, Holsten et Al. (Holsten et al., 2018), utilized oil as well as deionized water as the dielectric and observed greater MRR with water (Ho et al., 2007). Oil dielectric was also used by Mishra et al. (2018). The adversative consequence of TiC formation during machining in hydrocarbon dielectric is well known as explained in previous section (Chen et al., 1999; Holsten et al., 2018; Li et al., 2016). Greater MRR and lesser electrode wear were noticed with distilled water over kerosene oil (Fonda et al., 2008). There is an optimum concentration of added particles in dielectric fluid to improve MRR. Kolli and Kumar (Kolli & Kumar, 2014, 2019) varied B_4C powder content in dielectric and demonstrated that, MRR raised with the rise of B_4C powder content. This might be due to an earlier decompose of dielectric, which decreases insulating strength and leads to a greater MRR (Kolli & Kumar, 2015). Furthermore, addition of surfactant and graphite powder in dielectric meaningfully enhance MRR and, reduce tool wear rate (TWR), surface roughness (SR) and recast layer thickness (RLT) at different conditions. At beginning, MRR rises as the content of surfactant rises and then reduces with additional rise of surfactant content. Chow et al., (Chow, Yang, Lin and Chen, 2008), used a rotating disk copper electrode below the workpiece during micro-slit die-sink EDM of Ti-6A1-4V alloy. Pure water and SiC powder mix were utilized individually as dielectric where the content of SiC powder was 25 g/l. Pure water dielectric for Ti–6Al–4V provides greater MRR and lesser TWR and smaller expanding-slit by engaging negative polarity. SiC powder mixed water sources a greater electrode wear and expanding-slit but smaller burr than those of pure water. SiC powder in pure water increases conductivity. Consequently, breakdown voltage is lesser than that of pure water, which raise MRR. SiC powder in pure water encourages a bridge function and dispersion of discharge energy. This indicates that, there are some discharge routes occurrence in various time recesses in desired discharge period. Consequently, one desired discharge forms few discharge craters. Each discharging waveform has a unique influence in pure water and SiC powder mixed water dielectrics. The discharging waveform was steady with the input pulse in pure water, and on the other hand, responded waveforms were completely dissimilar to primary input pulse in SiC mixed water. Therefore, several discharging affects were generated from a single input pulse, which took place because of the dispersal of discharge energy. A series of situations may take place on how discharging energy dispersal is affected in SiC powder mixed water. The electrode gap in pure water is smaller and craters are larger for higher insulation of water. On the other hand, SiC powder in pure water may extend electrode gap ($Gap_w < Gap_{w+SiC}$) as SiC powder induces the bridging effect and reduces the insulation of water. Therefore, a discharge column was simply generated because of bridging effect and produced a smaller crater as a result of gap expansion and corresponding discharge waveform. Nonetheless, either the comparative movement in discharge gap or the flow of dielectric might disrupt the additional powder in the gap and vanishes the transient bridging as well as discharging column effect. The insulating state in dielectric was then recovered. The flowing powder in dielectric generates another bridging, discharging column and a smaller crater successively. The gap voltage waveform in discharge gap was noticeably reduced. Nevertheless, discharge column disappears again and insulating status in dielectric is recovered as explained details by Chow et al. (2008).

3.4. Material removal rate

Sivakumar and Gandhinathan (Sivakumar and Gandhinathan, 2013) found that MRR in die-sink EDM is primarily influenced by pulse-on-time and discharge current. On the contrary, the tool wear was highly

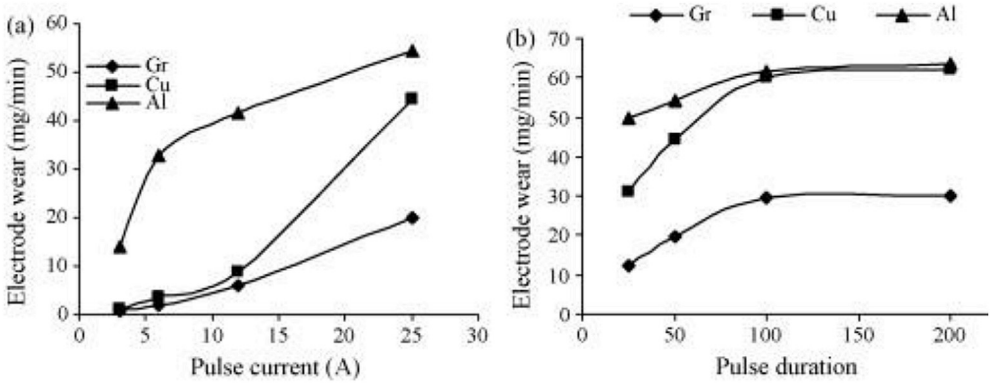

Figure 6. Electrode wear rate while die-sink EDM of titanium alloy: (a) 50 μs pulse-on-time and (b) 25 A peak current (Hasçalık and Çaydaş, 2007).

sensitive to varying pulse off and on-times, while the effect of discharge current is not significant. The over cut is generally dictated by the concentration of the discharge current as compared to the pulse off and on-times. Gu et al. (2012), considered different set of input parameters and mentioned that, dielectric flow rate, peak current and interactions between peak current and pulse on-time substantially contributes to varying MRR. The tool wear is pointedly influenced by the rate of dielectric flow and peak current in die-sinking EDM (Gu et al., 2012). Maximum working current of 25 A gives a highest MRR of 77.181 mm^3/min when graphite electrode was used. MRR rises as pulse-on-time rises until 200 μs and it decreases with additional increase of pulse-on-time (Hasçalık and Çaydaş, 2007). Removal of material during die-sink EDM of Ti6Al4V alloy does not take place at positive polarity of tool. This is due to the fact that, all discharge durations because of the generation of a TiC layer on the machined surface, acts as thermal barrier and thus, significantly impede material removal (Holsten et al., 2018). However, a tool negative polarity is feasible for this material as layer of TiC was comparatively thin and discontinuous in nature. This incipient of TiC layers are removed by greater power density occurrence on workpiece. The primary source of carbon accumulation is the oil dielectric instead of graphite tool electrode (Klocke et al., 2018).

3.5. Surface integrity

Positive polarity of tool electrode results in machined surface with cluster of cracks without any noticeable craters. However, negative polarity of tool produces surfaces with curved in craters without any apparent cracks. Formation of cracks is probably due to brittle/hard material classes on machined surface as result of anodic tool polarity. Ho et al. (2007), attained a varied recast layer thickness within ~4–11 μm, where rougher layer is obvious with positive polarity of tool electrode. Under tool negative polarity, recast layer was comparatively brighter, thinner and sporadic which (Ho et al., 2007) comprises a face-centered cubic (fcc) structure rich in carbon, indicating the presence of TiC. The size of grains of this layer was bigger for anodic tool polarity compare to that of cathodic polarity of tool (Holsten et al., 2018). The electrode materials also diffuse to machined surface. For example, Si and Cu were travelled from Cu–SiC electrode to workpiece and form $TiSi_2$ and TiC phases (Li et al., 2016).

Integrity of die-sink EDMed Ti6Al4V surfaces comprises roughening due to disintegration of recast layer, micro cracks, melted drops and debris (Nair et al., 2019). Just under the recast layer, a little tempered layer is also evident just like heat-affected zones (HAZ) in case of welded joints. The structure of such layer might be hexagonal martensitic (α′) depending on the cooling rate experienced by the material. Hardness of this layer is meaningfully greater than bulk because of $Ti_{24}C_{15}$ formation (Hasçalık and Çaydaş, 2007). In addition, diffusion of carbon also took place on EDMed Ti–6Al4V surface and henceforth, resulted higher micro-hardness due to carburization of the surface. The section of the machined surface is shown in Figure 7 (a) where the top-most layer is recast layer followed by marginally tempered layer and bulk material, correspondingly. Recast layer is generated by rapid solidification of unflushed molten material. This layer also specifies temperature dispersal experienced in workpiece throughout the process. Average thickness of recast layer rises as pulse-on-time rises at a persistent pulse current. It additionally rises meaningfully with the rise of pulse current at greater voltage and pulse-on-time as well as lesser flushing pressure and pulse-off-time (Verma and Sajeevan, 2015). The material of tool electrode obviously affects the thickness of recast and tempered layers. Density of surface cracks depends on average recast layer thickness where the thicker recast layer reduces density of surface crack. Surface cracks could be reduced at 3 and 6 A pulse currents for graphite and aluminum electrodes, correspondingly, while copper electrode generated surface cracks at all applied settings (Hasçalık and Çaydaş, 2007).

The machined surface, as shown in Figure 7 (b), comprises numerous miniscule unevenness related to spark between two electrodes, which causes globules of debris, pockmarks, craters, cracks etc. Figure 8 shows the influence of pulse current on titanium alloy surface generated from die-sink EDM. Greater discharging energy interrupts sparks and impulsive forces, which gives larger and deeper erosion craters as evident in Figure 8 (a). Figure 8 (b) presents a smoother surface compare to that in Figure 8 (a) due to lesser input current. Surface finish is directly related to peak voltage. Greater electric field is formed at high voltage and sparks happen easily, resulting rougher surface. Wire tension also contributes to surface finish where a smooth surface could be achieved at least vibration in wire which occurs at higher tension in wire. The surfaces generated by Cu–SiC electrode contains spark marks of larger radius, lesser cracks and harder recast layer than that by Cu electrode (Li et al., 2016).

Integral phenomena of EDM for example, arcing pulses, open circuit and short circuit, decrease the efficiency of sparking efficiency, which reduces overall performance. Efficiency of sparking is further decreased in drilling or cavity sink EDM because of recurrent short circuits occurrences in the existence of abundant debris in the spark gap. This necessitates active removal of debris from gap (Soni and Chakraverti, 1994). The main problems of die sink EDM are ineffective gap cooling and non-efficient flushing that induce collision or adhesion of molten precipitations on machined surface giving a thicker recast layer and mushy platelets (Soni, 1994). To overcome these limitations, side flushing is generally considered. Orbital motion of tool electrode is typically applied and rotation of tool electrode is ideal in drilling or micro EDM methods. Flushing through internal holes is characteristically applied for macro-hole-drilling methods (Gu et al., 2012).

The powder particles in dielectric are energized and move in a zigzag style when voltage is applied through the electrodes. Those produce a structure similar to that of a chain in spark gap, which bridges the gap. This also diminishes dielectric strength and gap voltage which start series of discharges. Frequency of spark increases as a result of flushing the debris efficiently away from the gap. This causes an active discharge transmissivity under sparking region because of raised thermal conductivity. Henceforth, MRR upsurges in powder mixed dielectric (Kolli &

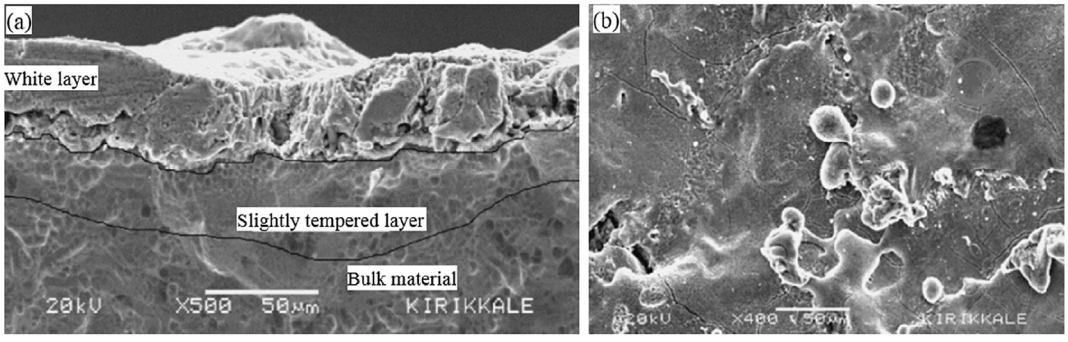

Figure 7. Die-sink EDMed titanium alloy (a) cross-section view under following machining condition: 6 A peak current, 100 μs pulse-on-time with graphite electrode (b) surface morphology view under following machining condition: 12 A peak current, 100 μs pulse-on-time with copper electrode (Hasçalık and Çaydaş, 2007).

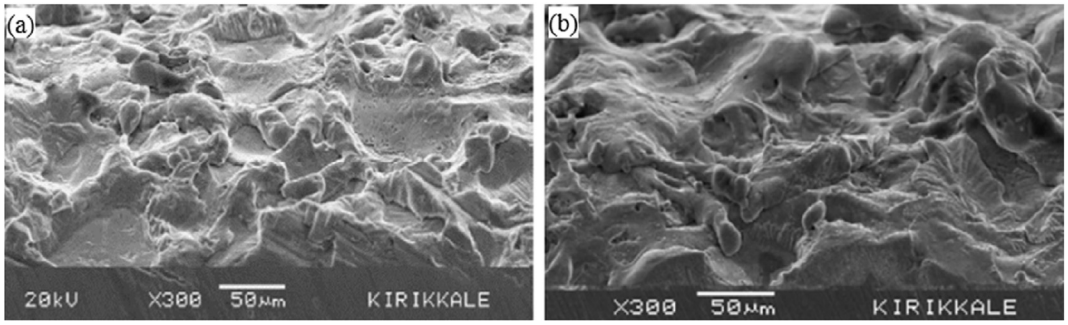

Figure 8. Die-sink EDMed titanium alloy surface at peak current of: (a) 25A and (b) 3A (Hasçalık and Çaydaş, 2007).

Kumar, 2015) and surface morphology contain irregular sizes of craters and debris which gives rougher surface. When graphite powder is incorporated, concentration of powder increases impulsive forces, and conductivity rise severely which give greater discharge energy density and gas explosions. At the start of gas explosion, materials breakdown and plasma zone extended, which increase surface roughness with larger and deeper craters. Tool wear rate decreases with the rise of 'span 20' surfactant and graphite concentration. However, recast layer thickness increases at first with the increase of these powder concentration and then reduces as powder concentration rises further (Kolli & Kumar, 2015). The application of bioactive hydroxyapatite powder suspension in dielectric cause calcium and phosphorus incorporation into recast layer. These elements improve hardness and induce anti-scratch properties on machined surface of pure titanium. Furthermore, hydroxyapatite suspension dielectric (5 g/L) generates smoother surface (Ra of 2.1 μm) and comparatively thin recast layer (~9 μm) with MRR of about 6.4×10^{-4} g/min during machining of titanium with grade-2 pure titanium rod electrodes and much lower compare to that in water dielectric. However, increasing hydroxyapatite content gradually rises recast-layer thickness, surface roughness, electrode wear rate, and MRR (Ou and Wang, 2017). The use of calcium chloride aqueous solution, during machining of titanium alloy with graphite electrode, produced calcium enriched uneven surface, in the form of titanium perovskite, which was credited to the incidence of re-solidification as well as ion embedding. A porous layer was noted on lateral section underneath a sample where an even hardened layer was generated up to a depth of around 200 μm from the surface (Sales et al., 2016).

4. EDM drilling

EDM also contributed towards increasing attention in producing micro-holes with greater aspect ratio in titanium alloy (Plaza et al., 2014). The modified version of die-sink EDM is EDM drilling where the diameter and length of holes are relatively smaller and larger, respectively. In this case, diameter of tool electrode varies from 0.1 to 10 mm (Gill and Singh, 2010; Tang and Du, 2014). EDM drilling penetrates considerably deeper at faster rates compared to nearly any other drilling process with the help of electrode guide and flushing effects. Drilling rates up to 1 mm/s can be attained with a diameter-to-length 1:150. This methods have been applied for creating holes in fuel injectors, turbine blades, coolant holes in cutting tool, medical equipment, plastic mold vent holes, hardened punch ejectors, and wire EDM starter holes (Yilmaz and Okka, 2010).

4.1. Mechanism

Similar to that of WEDM and die-sink EDM, mechanism of EDM drilling also depends on the behavior of workpiece material for example, high melting point and low thermal conductivity. Energy dispersal is significantly manipulated by power density on electrodes during drilling. Higher energy could be dispersed into electrodes at greater power density. The ratio of energy circulation decreases with the increase of discharge gap and pulse-on-time because of the enlargement of discharge plasma. In addition to spark gap and pulse-on-time, polarity is another crucial variable that can significantly influence energy dispersal features. Generally, higher energy is distributed in anode compare to that in cathode. The energy dispersal can also be influenced by geometrical form of electrodes (Shen et al., 2014).

Debris removal turns out to be serious matter during fabricating holes with elevated depth. Numerous methods have been adapted to improve debris removal, such as, rotating electrode, introducing dielectric through tool electrode and incorporation of backward time. A hole can be made by stationary as well as rotating electrode during EDM of Ti-alloy (Yadav and Yadava, 2015). The researchers have attempted to increase the effectiveness of stationary tool electrode EDM drilling by incorporating rotational motion of the tool electrode. Jeswani (1979) performed EDM by rotating tool electrode to drill smaller holes of 0.19–0.71 mm diameter in high carbon steel with a copper wire tool electrode. Similarly, Soni (Soni and Chakraverti, 1994) applied the technique to drill holes in titanium alloy by copper-tungsten electrode and noted that, MRR was higher for drilling through-holes than that of blind-hole at all rotating speeds. TWR raised with speed, however, TWR was not influenced noticeably. Wear of electrode corner and radius of hole corner in machined blind-holes were lesser with rotating electrode (Soni and Chakraverti, 1994). Yadav and Yadava (Yadav and Yadava, 2015) showed advantages of rotating tool electrode over static electrode for drilling holes on titanium alloy by varying tool rotation 300–800 rpm, duty factor of 11–15% and gap current of 66–74 A in oil based dielectric. Pure electrolytic copper (99.9 %) of 10 mm diameter was utilized as tool electrode in a high accuracy CNC machine tool. Surface roughness was found to rise as gap current and duty factor rises. Surface roughness was achieved in the range of 2.30–3.33 μm by rotating electrode; in contrast, stationary electrode gave surface roughness in the range of 2.50–3.50 μm. Increase of tool rotational speed improved the average hole circularity and smoothen the re-solidified layer. With a stationary electrode, obtained average hole circularity was between 36–43 μm, whereas with rotating electrode it was about 22–23 μm.

Yilmaz and Okka (Yilmaz and Okka, 2010) used single and multi-channel tubular rotating electrodes of brass and copper to drill holes in Ti–6Al–4V and noted that, electrode with single-channel gave greater MRR and lesser tool wear while electrode with multi-channel provided lower surface roughness. Brass electrode is more effective for achieving enhanced MRR. Single-channel brass electrode experienced lowermost wear as compared to others which might be due to higher thermal conductivity of brass and single channel got higher volumetric consumption of dielectric compare to that of multi-channel electrode. Multi-channel electrode provided better surfaces finish, which might be due to better flushing, influence of multi-channel electrode that takes away debris effectively, steadies' discharges, and controls the re-solidified process. Microstructural variations in machined surface of drilled holes change hardness that reduce gradually along the depth from

machined surface. Multi-channel electrode gave lesser range of hardness than that of single channel electrode.

Plaza et al. (2014), applied electrode rotation, backward time and helical shaped electrode to ease debris removal. Backward time was a programmed time when the electrode moved backwards and facilitated removal of debris. Helical-shaped electrodes also facilitated efficient flushing. Machining times were reduced by 37 % while having 45º helix angle and 50 μm flute-depth for 0.8 mm diameter CuW electrode. An additional 19 % reduction in machining time was achieved with the increase of flute-depth to 150 μm. All these improvements were due to efficient flushing and removal of debris. Due to system instability, helical geometry at the tip of electrode is not sustainable during whole operation time. Therefore, debris from both electrode and workpiece are not removed properly, and generate further instability that result in conical shape hole. This can be avoided by re-sharpening through EDM-cutting the broken tip in the same machine where drilling was done. Longer backward time could give holes with higher aspect ratio, but it requires more time. Electrode wear is not affected by backward time (Plaza et al., 2014).

4.2. Tool electrode

Different tool electrode materials such as, tungsten, copper-tungsten, graphite, brass and tungsten carbide were used during EDM drilling of titanium alloy (Alias et al., 2012; Azad and Puri, 2012; Mondol et al., 2015; Plaza et al., 2014). Plaza et al., (Plaza et al. (2014), reported that graphite as electrode accomplishes better compare to CuW in lower (under 0.15 mm) depth. MRR by graphite electrode decreases intensely and tool electrode wear raised as high as 400 % while drilling with depth beyond 0.5 mm. Copper electrodes undergo lower wear than brass because of greater melting temperature of copper compare to that of brass (Yilmaz and Okka, 2010) though brass electrode is more economical than copper and tungsten tools (Tiwary et al., 2015). CuW electrodes perform much better than graphite electrode for micro EDM drilling of high aspect-ratio holes in titanium alloy as 0.3 mm graphite electrodes experience 16 times more wear resistance compared to that of CuW electrodes to generate 0.5 mm hole (Plaza et al., 2014).

4.3. Dielectric fluid

Tap water, oil, deionized water, kerosene, and B_4C added dielectrics were used during EDM drilling of titanium alloy (Aligiri et al., 2010; Murahari & Kumar, 2014; Shen et al., 2014). Tap water offers reasonably high MRR with decreased machining cost without having any harmful effect on operators as well as environment (Tang and Du, 2014). MRR is greater with deionized water as dielectric compare to that of kerosene while EDM drilling of Ti–6Al–4V alloy using 300 μm diameter tungsten tool electrode. This is because of generation of oxide (TiO_2) layer on the machined surface in deionized water. This melts at lesser discharge energy compare to that of carbide (TiC) which is generated in kerosene dielectric. Though the addition of B_4C powder to kerosene does not improve MRR remarkably, B_4C powder in deionized water demonstrates an exceptional rise of MRR because of effective dispersal of discharge. Kerosene is decomposed at greater temperature by higher discharge energy and generates carbon which adheres to the surface of micro tool electrode and prevents quick tool wear, which is absent during the use of deionized water. Henceforth, TWR is greater in deionized water than that of kerosene. TWR is also higher in B_4C-mixed deionized water than that in kerosene. Overcut of micro-holes is small in lower discharge energy in deionized water compare to that in kerosene. Nevertheless, deionized water gives bigger overcut at greater discharge energy compare to that of kerosene. Subsequently, accurateness of micro hole is greater at lesser peak current and pulse on-time in deionized water and at greater peak current and pulse-on-time in kerosene dielectric. Both dielectrics mixed with B_4C powder give greater overcut compare to that of pure dielectrics. Experimental results showed that, DVEE (diameter variance at entry and exit hole) of produced micro holes is lesser in deionized water compare to that in kerosene dielectric. Nevertheless, larger peak current (1.5 and 2 A) gave greater DVEE in deionized water. Addition of B_4C powder in both dielectrics increased DVEE at lesser discharge current, but deionized water mixed with B_4C produces lesser DVEE at greater discharge energy as compared to that in pure deionized water. Recast layer formation is lesser in deionized water as compared to that in pure kerosene. The rise of pulse-on-time raises the thickness of recast layer in both the dielectrics. Formation of recast layer in B_4C powder mixed dielectric is relatively lower than that with pure deionized water or kerosene. This is because of more efficient removal of debris by pure dielectrics from the discharge gap. Deionized water and B_4C powder mixed deionized water dielectrics give smoother surfaces than those in kerosene and B_4C powder mixed kerosene respectively (Kibria et al., 2010).

4.4. Material removal rate

As reported by Mondol et al. (2015), MRR and TWR rise with the rise of capacitance while micro-drilling of titanium alloy. At 110 V voltage and 100 nF capacitance, MRR was highest. On the other hand, 130 V voltage and 100 nF capacitance gave highest TWR. The wear ratio (WR) was highest at 106 V voltage and 8 nF capacitance. The overcut was lowest at 130 V and 1 nF, and taper was lowest at 90 V and 1 nF. The voltage and capacitance should be between 95–120 V and 27–31 nF for highest MRR and least TWR, respectively. The ranges of voltage between 100 and 112 V, and capacitance between 25 and 40 nF were suitable for higher MRR and WR. The voltage and capacitance ranges should be 114–128 V and 12–25 nF, correspondingly, for greater MRR and lesser overcut. The ranges of voltage and capacitance should be 94–112 V and 14–20 nF, correspondingly least taper with highest MRR. Pulse-on and pulse-off-times do not noticeably affect MRR until certain depth of hole is achieved. However, MRR increases significantly with pulse-off time when depth of hole is beyond certain limit. On the other hand, tool wear increases significantly with pulse-on-time when the depth of drill is larger than certain value (Plaza et al., 2014). It was reported that deep cryogenic treatment of titanium 6246 alloy enhanced WR, MRR and lowered TWR (Gill and Singh, 2010). Tang and Du (Tang and Du, 2014) used red copper rod electrode of 10 mm diameter and 100 mm of length in tap water dielectric. With the change of machining parameters from (discharge current 11 A, ration of pulse-on to pulse-off-times 30/70 and gap voltage 30 V) to (discharge current 11 A, ration of pulse-on to pulse-off-times 50/50 and gap voltage 25 V), MRR increased from 1.28 to 2.38 mm^3/min, TWR reduced from 0.14 to 0.10 mm^3/min and SR reduced from 2.37 to 1.93 μm. The generated holes in these two conditions are shown in Figure 9. The machining variables sequenced in the order of comparative importance: the ratio of pulse-on to pulse-off-times, discharge current, lifting height and then gap voltage. Tiwari et al. (Tiwary et al., 2015), found that, optimum parameters for micro-EDM with 300 μm brass tool electrode in oil based dielectric during machining of Ti6Al4V are pulse-on-time of 1 μs, current of 2.5 A, voltage of 50 V, and wire tension of 0.20 kg/cm^2. Highest MRR attained was 0.0777 mg/min, and minimum TWR, OC, and taper was 0.0088 mg/min, 0.0765 mm, and 0.0013, correspondingly. The entry and exit of hole machined under these conditions were investigated. The edges of the hole were not perfectly smooth where the entry of the hole was cleaner than the exit of the hole apparently.

4.5. Surface integrity

Similar to other EDM processes, EDM drilling also generate rougher surface with recast layer. The holes and corresponding machined surfaces at diverse machining circumstances are presented by (Pradhan et al. (2008). No crack on machined was visible for machining condition considered but the appearance of machined surface is very similar to a typical surface achieved from any EDM process. Melted drops and craters are absent, pockmarks, and globules of debris are more obvious.

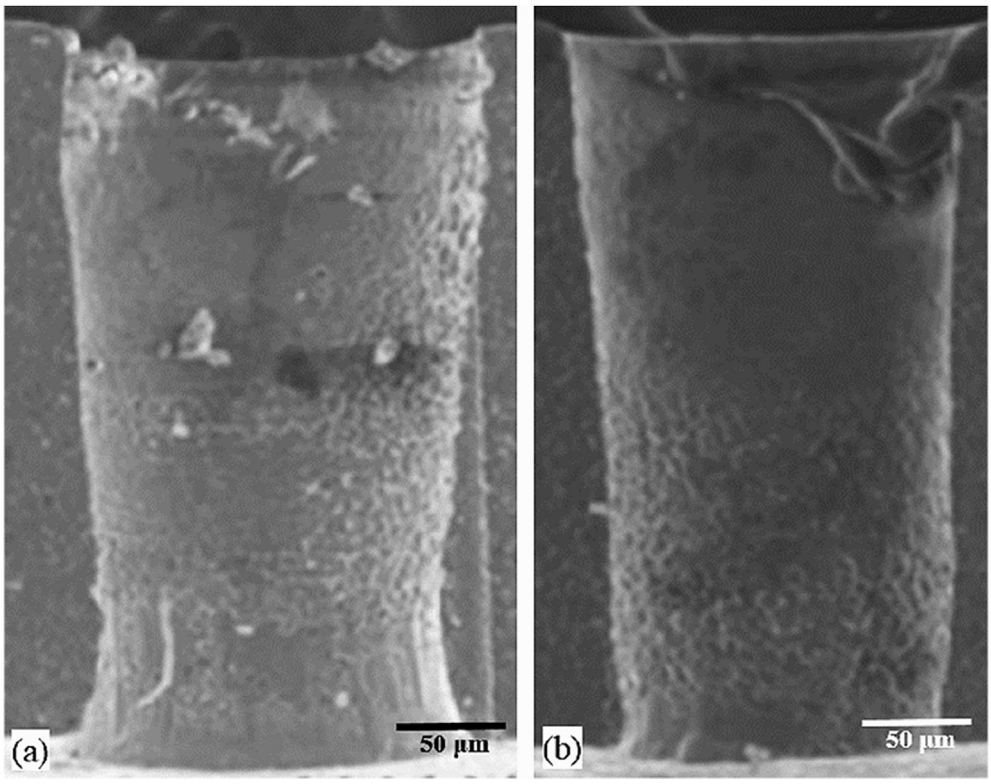

Figure 9. Side wall morphology of machined hole: (a) discharge current 11 A, pulse-on-time 30 μs, pulse-off-times 70 μs and gap voltage 30 V, and (b) discharge current 11 A, pulse-on-time 50 μs, pulse-off-time 50 μs and gap voltage 25 V (Tang and Du, 2014).

However, cracks in machined surface obtained by Yilmaz and Okka (2010), who also noticed that single-channel brass electrode generates a surface with larger melted drops and debris. The quality of surface formed by multi-channel brass electrodes was smoother with fewer cracks and debris. This could be described by better flushing of multi-channel electrode. It was reported that carbon and oxides particles are less in 0.5 A peak current, 20 μs pulse-on-time, 0.5 kg-cm^2 flushing pressure, 95% duty factor, which validates this machining condition produced minimum recast layer thickness (Pradhan et al., 2008). Microstructural variations (in SEM (Gorji et al., 2020)) in the HAZ of drilled holes cause the alteration of hardness that is progressively declining along the distance from machined surface. Multi-channel electrodes yield lower hardness compare to single-channel electrodes. EDM fast hole drilling procedures harden Ti–6Al–4V alloy (Yilmaz and Okka, 2010). While investigating the cross-section of surfaces at machining conditions (a) 0.5 A peak current, 1 μs pulse-on-time, 0.1 kg-cm^2 flushing pressure, 60% duty factor, (b) 0.5 A peak current, 10 μs pulse-on-time, 0.1 kg-cm^2 flushing pressure, 60% duty factor, and (c) 0.5 A peak current, 20 μs pulse-on-time, 0.5 kg-cm^2 flushing pressure, 95% duty factor condition, it was reported that carbon and oxides particles are more in conditions (b) and (c) compare to that of condition (a), which validates that machining condition of 0.5 A peak current, 1μs pulse-on-time, 0.1 kg-cm^2 flushing pressure and 60 % duty factor produce minimum recast layer thickness (Pradhan et al., 2008).

The increase of peak current and pulse-on-time rises the thickness of recast later. The increase of pulse-on-time rises the period of effective machining per cycle and melted material becomes re-solidified owing to partial flushing. It was established that the cavities are created at recast layer and rises with pulse-on-time and peak current. The surface of micro-hole becomes rougher as the pulse-on-time and peak current rise. The (Pradhan et al., 2008).

5. Hybrid processes

The hybrid machining process deals with the combinations of conventional EDM with one or two more processes to improve the overall machinability. Such a combined process aims at lowering the disadvantages associated with a specific process with the incorporation of an additional process. Ultrasonic, laser and magnetic field assisted EDM process has been successfully employed to improve the overall machinability of titanium alloy in EDM process.

5.1. EDM-ultrasonic

The work reported by Kremer et al. (Kremer et al., 1989; Kremer et al., 1991) were among the first pioneer to investigate the overall influence of a vibrating tool on the EDM process. The incorporation of a vibrating tool electrode resulted in higher material removal rate with improved surface finish. Furthermore, the authors reported that a proper synchronization of the discharges and the ultrasonic vibration of the tool electrode led to an all-round improvement of the machining capabilities. Chen et al. (Chen et al., 1997) identified that the incorporation of ultrasonic vibration during EDM of Ti–6Al–4V alloy resulted in improved material removal rate with better machined surfaces. The improvement in the overall machinability of titanium alloy in ultrasonic assisted electric discharge machining (USEDM) was mainly due to the restraining of discharges is a small/specified location thereby leading to formation of small debris. This in fact pertains to a more pronounced ejection of debris particle from the machining gap by the constantly moving dielectrics. Moreover, the severity of recast layer formation was reported to be comparatively lesser with the incorporation of ultrasonic vibration in EDM process.

Lin et al. (Lin et al., 2000) reported that the incorporation of USEDM with SiC as the abrasives, during machining of Ti–6Al–4V alloy resulted in a homogenous distribution of the debris particle throughout the discharge zone. This led to a better sparking and lesser arcing scenario. As a result, an improved machining rate was observed. Moreover, the use of distilled water as the dielectric fluid resulted in higher removal of the workpiece material as compared to kerosene. This is however with a compromise towards the measured surface roughness. Furthermore, a detailed analysis on the transverse section of the machined surface showed a thinner recast layer formation with USEDM in comparison with the conventional EDM process (Figure 10). The reduction in the recast layer formation is mainly due to the higher rate of molten material removal by the impinging abrasives and subsequent flushing actions. Finally, a detailed analysis of the influence of the abrasive particle size (3–9 μm) reported a better machining characteristic with smaller abrasive size in USEDM. Further, Zhang et al. (Zhang et al., 2012) reported that the incorporation of SiC abrasive particles in USED milling resulted in reduction of surface cracks as well on top of the previously reported improvement in surface finish and recast layer severity. Huang et al. (Huang et al., 2003) reported that the improvement in the machining rate with USEDM increased the tool wear as well. However, the net increase in the machining rate by more than 60 times outweighs the increased electrode wear. A threshold ultrasonic amplitude of 8 μm was reported in their work for effective machining. Any increment in the ultrasonic amplitude beyond 8 μm would led to a direct collision of the tool electrode and the workpiece material, ultimately terminating the machining process due to increased arcing and short-circuiting. Such a situation can be effectively controlled by properly coordinating the ultrasonic amplitude with the spark gap and the associated servo mechanism. Similar inference of reduction in arcing/short-circuiting and increase in normal discharges was also reported by Shabgard and Alenabi (Shabgard and Alenabi, 2015) with the application of USEDM process. Moreover, it was further reported that USEDM was more beneficial in lower pulse energies with regards to surface characteristic improvements and reduction in thermal damages than higher pulse energies, as compared to the conventional EDM process. It seems that the debris evacuation and flow of dielectric are optimized at lower pulse energy.

Furthermore, Khosrozadeh and Shabgard (Khosrozadeh and Shabgard, 2017) made a comparison of the overall machinability of the USEDM with conventional EDM, powder mixed EDM (PMEDM) and ultrasonic assisted powder mixed EDM (PM-USEDM). A more pronounced machining with better surface profile was observed with PM-USEDM as compared to other techniques. The severity of surface cracks and thermal damage were observed to gradually reduce with USEDM, PMEDM and PM-USEDM processes as compared to conventional EDM. Further, the thermal damage was observed to reduce by almost four times with the incorporation of PM-USEDM as compared to conventional EDM process. This substantially reduces the overall cost that has to be incurred towards polishing of the machined surface. Similar inference was reported by Yunpeng et al. (Yunpeng et al., 2014) during machining of titanium alloy with Al and SiC powder as the abrasives. A reduction in surface roughness, recast layer and residual stresses was observed in comparison with the normal EDM and PMEDM.

Tsai et al. (Tsai et al., 2018) tried to identify the influence of tool electrode materials on the overall machinability during USEDM grooving of Ti–6Al–4V alloy. For this, three different types of electrode were considered viz. copper (Cu), copper-tungsten (Cu–W) and graphite. The machinability was found to improve with the application of ultrasonic vibration with Cu and Cu–W as the tool electrodes due to the increased flushing of the molten materials. However, a reverse behavior was observed when machined with graphite as the tool electrode. This inference was reported to be caused by strong layered atomic structure of the graphite electrode which causes slag adsorption, thereby lowering the effectiveness of the induced vibration. Another possible explanation as stated by Hasçalık and Çaydaş (Hasçalık and Çaydaş, 2007) is the formation of a hard TiC carbide layer on the machined surface, which has a melting point of 3150 °C (twice that of Ti). As a result, an intense amount of energy is required to break/melt the surface material. This justification was in accordance with the variation in machining capabilities of Ti alloy with Cu and Cu–W as tool to that of graphite tool for a specific EDM parameters.

5.2. Ultrasonic μ-EDM

The application of ultrasonically vibrating tool electrode in μ-EDM process paved a way to facilitate deep and small hole drilling of Titanium alloys which was initially a difficult method owing to the low thermal conductivity and high tenacity (Wansheng et al., 2002). The high

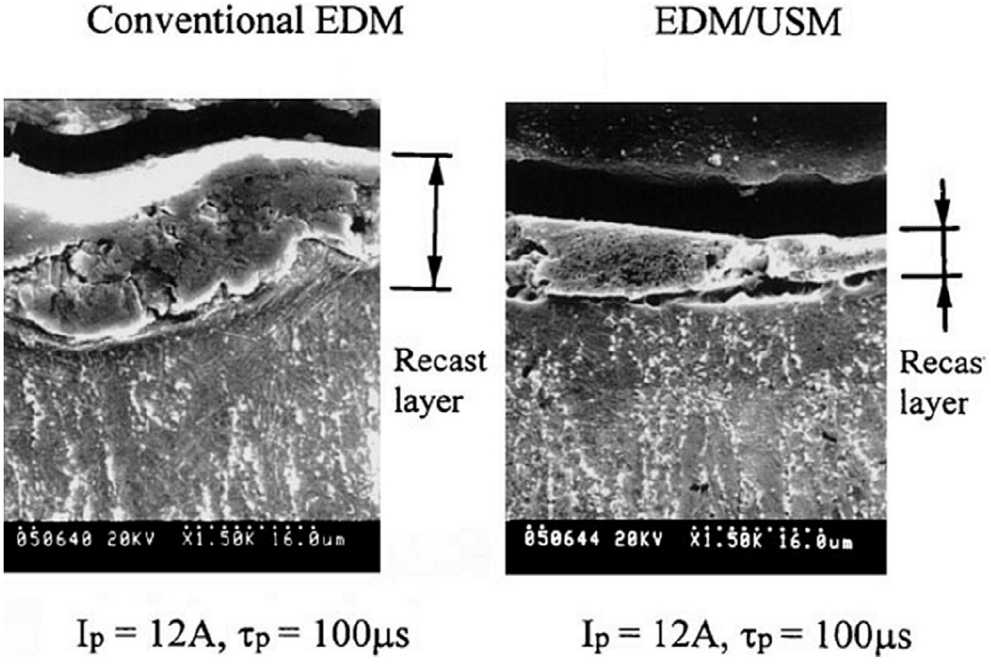

Figure 10. Typical SEM micrographs of the recast layer (Lin et al., 2000).

frequency alternating press shock wave generated in ultrasonic assisted micro electrical discharge machining (μ-USEDM) induces a high liquid pressure difference in the machining zone. This substantially improves the flow behavior of the liquid, thereby lowering the probability of accumulation of debris particle around the machining zone. As a result, the arcing phenomena reduces considerably, thereby enhancing the overall machining stability and effectiveness. Moreover, the cavitation effect produced in μ-USEDM favors re-boiling of the fused material in the eroded crater due to the rapid drop in the pressure. This in turn, facilitates ejection of the fused metal, thereby lowering the liquid metal re-solidification on the machined surface. Thus, such a scenario ultimately leads to effective drilling of deep and small holes with lesser severity of recast layer formation. Figure 11 shows the comparison of the capability of drilling deep micro holes of Ti–6Al–4V using μ-EDM and μ-USEDM process. As observed from the figure, μ-EDM fails severely to drill high aspect ratio holes due to intense electrode wear, while successful micro drilling was observed with μ-USEDM. Moreover, the single notch type electrode yielded a faster machining rate as compared to the circular shape electrode during μ-USEDM. This is mainly due to the increased space for debris particle flow in the machining zone, which increases the overall efficiency while minimizing the taper as well.

Similar inference was also reported by Mastud et al. (Mastud et al., 2014) during reverse μ-USEDM to generate high aspect ratio micro textures and micro arrays. The successful fabrication was achieved due to the enhanced dispelling of debris particle from the machining zone with the incorporation of a vibrating tool. Further, it was observed that increasing the frequency and the amplitude of the tool electrode vibration impedes a higher average velocity of the eroded debris particle. This is mainly due to the higher momentum imparted to the debris with an increase in the velocity of the electrode. In their work, a maximum particle velocity of 2.1 m/s was observed with a frequency of 6 kHz as against 0.81 m/s and 0.59 m/s for 1 kHz and stationary electrode. Moreover, the detailed voltage current characteristics depicted reduction in arcing/short-circuit scenario, indicating lower debris agglomeration, thereby leading to an improved process stability. In continuation of the work, Singh et al. (Singh et al., 2018) performed a detailed parametric analysis in μ-USEDM of Ti alloy using tungsten carbide as the electrode. The MRR was observed to be positively influenced by pulse current, pulse-on-time and ultrasonic power. Further, it was reported that for a particular EDM parameter, the tool wear and the taper angle of the drilled hole decreases gradually with an increase in the ultrasonic power. This is mainly due to effective flushing and debris removal with an increase in the ultrasonic vibration. Moreover, the machined surface of the drilled hole was observed to possess a small amount of recast layer due to the increased flushing capabilities with the application of a vibrating micro tool.

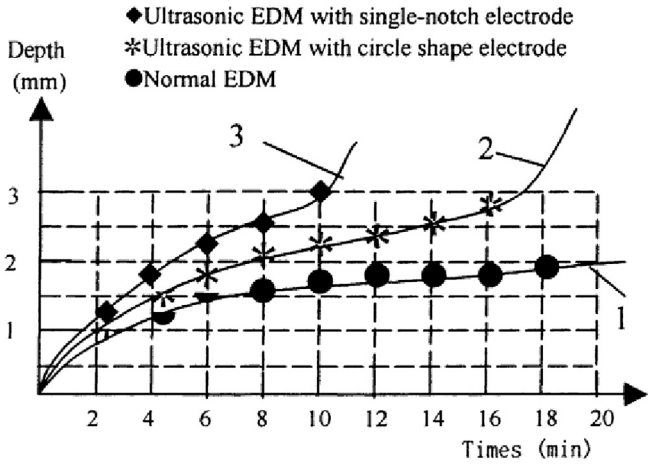

Figure 11. Capabilities of high aspect ratio micro-drilling of Ti–6Al–4V alloys (Wansheng et al., 2002).

5.3. Laser-EDM

The major disadvantage associated with micro-EDM process is the incapability to remove material at a very high rate. While, laser machining suffers greatly on the machined surface characteristics. The combined laser-EDM process as reported by Al-Ahmari et al. (Al-Ahmari et al., 2016) focuses on lowering the disadvantage associated with the individual processes. The hybrid technique focuses on initial drilling using a Nd:YAG laser of wavelength 1064nm, and subsequent finishing using a μ-EDM process, with varying parametric combination. Here, an initial laser drilling was performed over a diameter of ~150 μm. Further, the laser processed hole were EDMed with a brass tool of diameter 200 μm. The hybrid process resulted in reduction of the taper angle due to the reduced nature of tool wear rate and higher flushing capabilities. Moreover, the machining time was reported to reduce by ~65% as compared to the normal μ-EDM process. The improved machining rate was observed to be mainly influenced by the reduction in short-circuiting and arcing scenario in the hybrid process which facilitates a faster travel of the tool electrode towards the workpiece.

5.4. Magnetic field assisted EDM

Heinz et al. (Heinz et al., 2011) reported a novel technique to improve the machinability of non-magnetic material (Ti Grade 5) in micro EDM by incorporating an additional magnetic field in the machining zone. The magnetic field in the machining zone had a direct influence on the plasma and debris particles due to the generated Lorentz force. A proper control of the orientation of the Lorentz force along the work piece surface resulted in shifting of the debris particle to a greater distance from the melt pool. This facilitates a better removal of work piece material due to the increased flushing by the induced mechanical effect. An improvement of the material removal by almost 50% was reported by the authors in their analysis.

6. Thermal modelling for EDM of Ti alloys

The method of numerically predicting the erosion mechanism of titanium alloy in EDM process was first carried out by Xie et al. (Xie et al., 2011). The simulation was based on a single spark model formulated by Dibitonto et al. (Dibitonto et al., 1989) and Patel et al. (Patel et al., 1989). The heaty affected zone was positively influenced by increase in the discharge current and pulse duration. The incorporation of latent heat resulted in reduction of the peak temperature in the machining zone. This is mainly due to the associated losses of heat energy to change the state of workpiece from solid to liquid and liquid to gas. The results predicted by the numerical simulation was observed to be in appreciable agreement with the experimental results. Similar inference was also reported by Liu et al. (Liu et al., 2014) during machining of TC4 in EDM process. Further, the authors reported that they were able to predict the results with an error of around ~10 % only. Kuriachen et al. (Kuriachen et al., 2015) tried to predict the overall temperature and crater profile during μ-EDM of titanium alloy. A higher temperature profile was observed with an increase in the voltage and capacitance. A single discharge experimental validation showed a fairly similar trend of the crater profile observed in the numerical simulation. However, the numerically obtained crater profile had a comparatively larger spread. This was mainly due to the assumption that the plasma flushing efficiency is 100 %. On the other hand, during actual experimentation, a portion of the melted materials gets re-solidified instantaneously, which ultimately pertains to a smaller spread as compared with the numerically obtained profile.

Mujumdar et al. (Mujumdar et al., 2015) made an improvement in modelling of material removal behaviour of titanium alloy by considering the melt-pool, heat transfer and fluid flow characteristics. A

two-stage method was considered by the authors to perform the analysis. The plasma heat flux, pressure and bubble radius obtained from the plasma model are used as the input variables in the melt-pool model to identify the net material removal from the surface of the workpiece. The numerical results were observed to predict the crater diameter in close proximity with that of the actual experimental results. However, the model over-predicted the crater depth. Such a behavior was reported to be mainly influenced by the partial ejection of the melted materials and subsequent re-solidification.

The occurrence of residual stresses post-EDM process is inevitable due to the thermal phenomenon associated with the material removal mechanism. A detailed analysis will yield a step closer towards minimization of the defects. Tang et al. (Tang and Yang, 2018) modelled a single discharge crater profile to identify the extent of thermal phase transformation on the machined surface and its subsequent residual stress distribution. The Von Mises stresses was reported to initially increase rapidly and then decreases with an increase in the depth. Moreover, the stress concentration was observed to be maximum around the center of the profile, and gradually decreases towards the periphery of the discharge crater. The model predicted a maximum stress value at the interface of the recast layer and heat affected zone, depicting the interface region as the most vulnerable region to large plastic deformation. A detailed analysis of the stress tensor depicts simultaneous compressive as well as tensile stress component in the recast layer. Furthermore, the stress behavior was reported to be highly influenced by the pulse duration and discharge current, which increases with a corresponding increase in the above-mentioned parameters. Thus, the numerical analysis could pertain to be an effective tool in identifying the depth of surface material that has to be polished after EDM. Similar variation in the simulated residual stress was observed by Murali and Yeo (Murali and Yeo, 2005) as well, with maximum stresses around the crater center. Moreover, the simulated stresses agree with the experimentally obtained stresses using atomic force microscope and nanoindentation technique.

The movement of the debris particle and subsequent flow behavior in the machining gap is an important aspect to relate deep hole drilling of Ti alloys in EDM process. Zhang et al. (2017) developed a two phase (solid-liquid) flow model with flushing and self-adaptive desaturation concept. The variation in the velocity field, pressure field and debris particle motion were identified numerically in the gap. The incorporation of flushing depicted a gradual movement of the debris particle from the machining zone. This lowers the probability of arcing in the machining zone, thereby improving the overall process. Further increase in the flushing velocity had a positive impact on the overall debris particle removal. Similar inferences were also observed with varying pressure field as well. However, the capability of efficient debris removal reduces with an increase in the machining depth. During the expulsion of debris from deep holes, there is an increased probability of discharges occurring on the side wall by the traversing debris. This pertains to the taper behavior which was observed in actual experiments as well. Moreover, the presence of burn marks at the bottom of the drilled holes depicted actual clustering of debris, thereby leading to arcing phenomena.

The concept of numerical formulations with regards to USEDM was laid forward by Kong et al. (Kong et al., 2015) and Mastud et al. (Mastud et al., 2015) by analyzing the debris and flow behavior during machining of titanium alloy. Kong et al. (2015) numerically compared the nature of bubble formation and corresponding motion in the machining zone with and without the application of ultrasonic vibration. The improvement in the overall machinability with USEDM was observed numerically due to the increased bubble concentration in the machining domain. This in turn, correlates to a more pronounced expulsion mechanism of the debris and molten materials. Similar observation was also laid forward by Mastud et al. (2015) as well by thoroughly analyzing the debris motion and dielectric flow behavior, both experimentally and numerically. The increase in the ultrasonic frequency and amplitudes led to a higher debris motion and flow behavior which directly allied to an increased machining capability.

7. Future aspects

Titanium alloy is relatively expensive and specially used in aerospace and biomedical applications due to its exceptionally desired properties. Titanium alloys parts have to be defect free for those applications and those parts are mainly produced from traditional machining process. Though there are some advantages of non-traditional processes over traditional methods for example, lower cost and ease of making complex shapes, but traditional machining process changes the properties of machined surface unexpectedly without any proper control.

Despite huge research interests in this field, many research challenges are still unsolved. Innovative procedures are being established, and the present techniques necessitate an inclusive understanding of the enhancements of properties of products and procedures for example, productivity, performance, life expectancy, sustainability, robustness, flexible automation, etc. It is anticipated to detect some vital research areas needed for future expansion to attain anticipated processes and products as given below:

- Development of models to predict the performance of EDM techniques.
- Reference guidelines for impartial valuation and performance assessment of existing methods side by side.
- Further progresses of hybrid methods by merging several methods so that the demerits of distinct methods are minimized, and merits of distinct methods are super positioned to augment machining performance.

8. Conclusions

The highly desired properties of titanium alloy induce added complexity and make machining procedure more challenging compare to that of common materials. The EDM procedures have diverse arrangements of removing materials by using different types and materials of tool electrode, dielectric fluid and machining parameter. However, mechanism of material removal is similar in different EDM processes where electric arc generated at the vicinity of the workpiece. This generate high heat which melts and vaporises the workpiece along the path of tool electrode movement. The machined surfaces generated from EDM processes consist of cracks, recast layer, residual stress and heat affected zone due to high temperature generation, low thermal conductivity and high cooling rate.

WEDM is the most commonly used EDM process due to its versatility due to a range of choices of tool wire materials and environment friendly dielectric fluids (e.g., de-ionized or distilled water). In addition, as the wire travels continuously the effect of tool wear is less on the machined features. However, the flexibility of the wire electrode contributes to dimensional accuracy and machining performance. The MRR in this process can be as high as 33.6 mm^3/min.

In die-sinking EDM, a rigid tool electrode of different materials such as, graphite, aluminum, copper, etc. is used depending on the requirements of surface finish and material removal rate. The wear of tool electrode affects the geometric accuracy reasonably. Mainly hydrocarbon dielectrics are used for titanium alloys which contributes to form TiC in the recast layer. The MRR in this method can be as high as 77.181 mm^3/min.

EDM drilling is mainly used to drill micro-holes of high aspect ratio. The tool electrode materials in this case are very similar to those of die-sinking EDM. Tap water, oil, deionized water, kerosene, and B_4C added dielectrics are used during EDM drilling of titanium alloy. Debris removal is the main challenge in this case which can be improved by rotating electrode, introducing dielectric through tool electrode and incorporation of backward time. The MRR is very low which is around 2.38 mm^3/min.

Several hybrid EDM methods are introduced to avoid problems in different methods. There are still deficiencies in techniques to control

output parameters as required. Recast layer, tool breakage and tool wear are key problems in EDM. Though there are techniques to avoid recast layer formation, these are very slow processes and yet to use in practical fields. Different hybrid EDM techniques have been introduced to improve the performance but the full benefit from all these techniques is yet to be exploited.

Declarations

Author contribution statement

All authors listed have significantly contributed to the development and the writing of this article.

Funding statement

This research did not receive any specific grant from funding agencies in the public, commercial, or not-for-profit sectors.

Competing interest statement

The authors declare no conflict of interest.

Additional information

No additional information is available for this paper.

References

Al-Ahmari, A., Rasheed, M.S., Mohammed, M.K., Saleh, T., 2016. A hybrid machining process combining Micro-EDM and laser beam machining of Nickel–Titanium-Based shape memory alloy. Mater. Manuf. Process. 31 (4), 447–455.

Alias, A., Abdullah, B., Abbas, N.M., 2012. Influence of machine feed rate in WEDM of titanium Ti-6Al-4 V with constant current (6A) using brass wire. Procedia Eng. 41, 1806–1811.

Aligiri, E., Yeo, S., Tan, P., 2010. A new tool wear compensation method based on real-time estimation of material removal volume in micro-EDM. J. Mater. Process. Technol. 210 (15), 2292–2303.

Alshemary, A., Pramanik, A., Basak, A., Littlefair, G., 2018. Accuracy of duplex stainless steel feature generated by electrical discharge machining (EDM). Measurement 130, 137–144.

Amorim, F.L., Stedile, L.J., Torres, R.D., Soares, P.C., Laurindo, C.A.H., 2014. Performance and surface integrity of Ti6Al4V after sinking EDM with special graphite electrodes. J. Mater. Eng. Perform. 23 (4), 1480–1488.

Antar, M., Soo, S., Aspinwall, D., Cuttell, M., Perez, R., Winn, A., 2010. WEDM of Aerospace Alloys Using 'clean Cut'generator Technology. ISEM XVI, Shanghai, pp. 285–290.

Aspinwall, D., Soo, S., Berrisford, A., Walder, G., 2008. Workpiece surface roughness and integrity after WEDM of Ti–6Al–4V and Inconel 718 using minimum damage generator technology. CIRP Ann. - Manuf. Technol. 57 (1), 187–190.

Azad, M., Puri, A., 2012. Simultaneous optimisation of multiple performance characteristics in micro-EDM drilling of titanium alloy. Int. J. Adv. Manuf. Technol. 61 (9-12), 1231–1239.

Chen, S., Huang, F., Suzuki, Y., Yan, B., 1997. Improvement of material removal rate of Ti-6Al-4V alloy by electrical discharge machining with multiple ultrasonic vibration. Keikinzoku 47 (4), 220–225.

Chen, S., Yan, B., Huang, F., 1999. Influence of kerosene and distilled water as dielectrics on the electric discharge machining characteristics of Ti–6A1–4V. J. Mater. Process. Technol. 87 (1-3), 107–111.

Chow, H., Yan, B., Huang, F., 1999. Micro slit machining using electro-discharge machining with a modified rotary disk electrode (RDE). J. Mater. Process. Technol. 91 (1-3), 161–166.

Chow, H.-M., Yang, L.-D., Lin, C.-T., Chen, Y.-F., 2008. The use of SiC powder in water as dielectric for micro-slit EDM machining. J. Mater. Process. Technol. 195 (1-3), 160–170.

Devarajaiah, D., Muthumari, C., 2018. Evaluation of power consumption and MRR in WEDM of Ti–6Al–4V alloy and its simultaneous optimization for sustainable production. J. Braz. Soc. Mech. Sci. Eng. 40 (8), 400.

Dibitonto, D.D., Eubank, P.T., Patel, M.R., Barrufet, M.A., 1989. Theoretical models of the electrical discharge machining process .1. A simple cathode erosion model. J. Appl. Phys. 66 (9), 4095–4103.

Fonda, P., Wang, Z., Yamazaki, K., Akutsu, Y., 2008. A fundamental study on Ti–6Al–4V's thermal and electrical properties and their relation to EDM productivity. J. Mater. Process. Technol. 202 (1-3), 583–589.

Ghodsiyeh, D., Lahiji, M.A., Ghanbari, M., Shirdar, M.R., Golshan, A., 2012. Optimizing material removal rate (MRR) in WEDMing titanium alloy (Ti6Al4V) using the Taguchi method. Res. J. Appl. Sci. Eng. Technol. 4 (17), 3154–3161.

Gill, S.S., Singh, J., 2010. Effect of deep cryogenic treatment on machinability of titanium alloy (Ti-6246) in electric discharge drilling. Mater. Manuf. Process. 25 (6), 378–385.

Gorji, N.E., Saxena, P., Corfield, M., Clare, A., Rueff, J.-P., Bogan, J., O'Connor, R., 2020. A new method for assessing the utility of powder bed fusion (PBF) feedstock. Mater. Char. 161, 110167.

Gu, L., Li, L., Zhao, W., Rajurkar, K., 2012. Electrical discharge machining of Ti6Al4V with a bundled electrode. Int. J. Mach. Tool Manufact. 53 (1), 100–106.

Hasçalık, A., Çaydaş, U., 2007. Electrical discharge machining of titanium alloy (Ti–6Al–4V). Appl. Surf. Sci. 253 (22), 9007–9016.

Heinz, K., Kapoor, S.G., DeVor, R.E., Surla, V., 2011. An investigation of magnetic-field-assisted material removal in micro-EDM for nonmagnetic materials. J. Manuf. Sci. Eng. 133 (2).

Ho, S., Aspinwall, D., Voice, W., 2007. Use of powder metallurgy (PM) compacted electrodes for electrical discharge surface alloying/modification of Ti–6Al–4V alloy. J. Mater. Process. Technol. 191 (1-3), 123–126.

Holsten, M., Koshy, P., Klink, A., Schwedt, A., 2018. Anomalous influence of polarity in sink EDM of titanium alloys. CIRP Annals.

Huang, H., Zhang, H., Zhou, L., Zheng, H., 2003. Ultrasonic vibration assisted electro-discharge machining of microholes in Nitinol. J. Micromech. Microeng. 13 (5), 693.

Jeswani, M., 1979. Small hole drilling in EDM. Int. J. Mach. Tool Des. Res. 19 (3), 165–169.

Khosrozadeh, B., Shabgard, M., 2017. Effects of hybrid electrical discharge machining processes on surface integrity and residual stresses of Ti-6Al-4V titanium alloy. Int. J. Adv. Manuf. Technol. 93 (5-8), 1999–2011.

Kibria, G., Sarkar, B., Pradhan, B., Bhattacharyya, B., 2010. Comparative study of different dielectrics for micro-EDM performance during microhole machining of Ti-6Al-4V alloy. Int. J. Adv. Manuf. Technol. 48 (5-8), 557–570.

Klocke, F., Holsten, M., Hensgen, L., Klink, A., 2014. Experimental investigations on sinking-EDM of seal slots in gamma-TiAl. Procedia CIRP 24, 92–96.

Klocke, F., Mohammadnejad, M., Holsten, M., Ehle, L., Zeis, M., Klink, A., 2018. A comparative study of polarity-related effects in single discharge EDM of titanium and iron alloys. Procedia CIRP 68, 52–57.

Klocke, F., Welling, D., Dieckmann, J., 2011. Comparison of grinding and wire EDM concerning fatigue strength and surface integrity of machined Ti6Al4V components. Procedia Engin. 19, 184–189.

Kolli, M., Kumar, A., 2014. Effect of boron carbide powder mixed into dielectric fluid on electrical discharge machining of titanium alloy. Procedia Mater. Sci. 5, 1957–1965.

Kolli, M., Kumar, A., 2015. Effect of dielectric fluid with surfactant and graphite powder on Electrical Discharge Machining of titanium alloy using Taguchi method. Engin. Sci. Techn, Int. J. 18 (4), 524–535.

Kolli, M., Kumar, A., 2019. Assessing the influence of surfactant and B 4 C powder mixed in dielectric fluid on EDM of titanium alloy. Siliconindia 11 (4), 1731–1743.

Kong, W.J., Guo, C., Zhu, X.J., 2015. Simulation analysis of bubble motion under ultrasonic assisted Electrical Discharge Machining. In: Du, W., Zhou, X. (Eds.), Proceedings of the 2015 3rd International Conference on Machinery, Materials and Information Technology Applications, 35, pp. 1728–1731.

Kremer, D., Lebrun, J., Hosari, B., Moisan, A., 1989. Effects of ultrasonic vibrations on the performances in EDM. CIRP Annals 38 (1), 199–202.

Kremer, D., Lhiaubet, C., Moisan, A., 1991. A study of the effect of synchronizing ultrasonic vibrations with pulses in EDM. CIRP Annals 40 (1), 211–214.

Kumar, A., Mandal, A., Dixit, A.R., Das, A.K., 2018. Performance evaluation of Al2O3 nano powder mixed dielectric for electric discharge machining of Inconel 825. Mater. Manuf. Process. 33 (9), 986–995.

Kumar, S., Khan, M.A., Muralidharan, B., 2019. Processing of titanium-based human implant material using wire EDM. Mater. Manuf. Process. 34 (6), 695–700.

Kuriachen, B., Varghese, A., Somashekhar, K.P., Panda, S., Mathew, J., 2015. Three-dimensional numerical simulation of microelectric discharge machining of Ti-6Al-4V. Int. J. Adv. Manuf. Technol. 79 (1-4), 147–160.

Laxman, J., Raj, K.G., 2014. Optimization of EDM process parameters on titanium super alloys based on the grey relational analysis. Int. J. Eng. Res. 3 (5), 344–348.

Lee, S., Li, X., 2001. Study of the effect of machining parameters on the machining characteristics in electrical discharge machining of tungsten carbide. J. Mater. Process. Technol. 115 (3), 344–358.

Lenin, S.D., Uthirapathi, A., Venkata, R.R.P.S., Durai Selvam, M., 2014. Influence of pulse-on-time on the performance of wire electrical discharge machining of Ti-6Al-4V using zinc coated brass wire. Appl. Mech. Mater. 592–594, 416–420.

Li, L., Feng, L., Bai, X., Li, Z., 2016. Surface characteristics of Ti–6Al–4V alloy by EDM with Cu–SiC composite electrode. Appl. Surf. Sci. 388, 546–550.

Lin, Y.C., Yan, B.H., Chang, Y.S., 2000. Machining characteristics of titanium alloy (Ti–6Al–4V) using a combination process of EDM with USM. J. Mater. Process. Technol. 104 (3), 171–177.

Liu, Y., Zhang, W.C., Zhang, S.F., Sha, Z.H., 2014. The simulation research of tool wear in small hole EDM machining on titanium alloy. In: Qiang, L. (Ed.), Advanced Development in Automation, Materials and Manufacturing, 624, pp. 249–254.

Mahardika, M., Tsujimoto, T., Mitsui, K., 2008. A new approach on the determination of ease of machining by EDM processes. Int. J. Mach. Tool Manufact. 48 (7-8), 746–760.

Mastud, S.A., Kothari, N.S., Singh, R.K., Joshi, S.S., 2014. Modeling debris motion in vibration assisted reverse micro electrical discharge machining process (R-MEDM). Journal of Microelectromechanical Systems 24 (3), 661–676.

Mastud, S.A., Kothari, N.S., Singh, R.K., Joshi, S.S., 2015. Modeling debris motion in vibration assisted reverse micro electrical discharge machining process (R-MEDM). J. Microelectromech. Syst. 24 (3), 661–676.

Mishra, D.K., Datta, S., Masanta, M., 2018. Effects of tool electrode on EDM performance of Ti-6Al-4V. Siliconindia 1–15.

Mondol, K., Azad, M., Puri, A., 2015. Analysis of micro-electrical discharge drilling characteristics in a thin plate of Ti–6Al–4 V. Int. J. Adv. Manuf. Technol. 76 (1-4), 141–150.
Mujumdar, S.S., Curreli, D., Kapoor, S.G., Ruzic, D., 2015. Modeling of melt-pool formation and material removal in micro-electrodischarge machining. J. Manuf. Sci. Engin.-Trans. Asme 137 (3).
Mukherjee, R., Chakraborty, S., 2012. Selection of EDM process parameters using biogeography-based optimization algorithm. Mater. Manuf. Process. 27 (9), 954–962.
Mukherjee, R., Chakraborty, S., Samanta, S., 2012. Selection of wire electrical discharge machining process parameters using non-traditional optimization algorithms. Appl. Soft Comput. 12 (8), 2506–2516.
Murahari, K., Kumar, A., 2014. Effect of additives added in dielectric fluid on electrical discharge machining of titanium alloy. In: Proceedings of the ICARMMIEM, p. 52e59.
Murali, M.S., Yeo, S.H., 2005. Process simulation and residual stress estimation of micro-electrodischarge machining using finite element method. Jpn. J. Appl. Phy. Part 1-Regular Papers Brief Communications & Review Papers 44 (7A), 5254–5263.
Nair, S., Dutta, A., Giridharan, A., 2019. Investigation on EDM machining of Ti6Al4V with negative polarity brass electrode. Mater. Manuf. Process. 34 (16), 1824–1831.
Nourbakhsh, F., 2012. Machining Stability of Wire EDM of Titanium.
Nourbakhsh, F., Rajurkar, K.P., Malshe, A.P., Cao, J., 2013. Wire electro-discharge machining of titanium alloy. Procedia CIRP 5, 13–18.
Ou, S.-F., Wang, C.-Y., 2017. Effects of bioceramic particles in dielectric of powder-mixed electrical discharge machining on machining and surface characteristics of titanium alloys. J. Mater. Process. Technol. 245, 70–79.
Pandey, A.K., Dubey, A.K., 2012. Simultaneous optimization of multiple quality characteristics in laser cutting of titanium alloy sheet. Optic Laser. Technol. 44 (6), 1858–1865.
Patel, M.R., Barrufet, M.A., Eubank, P.T., Dibitonto, D.D., 1989. THEORETICAL-MODELS OF the electrical-discharge machining process .2. The anode erosion model. J. Appl. Phys. 66 (9), 4104–4111.
Pilligrin, J.C., Asokan, P., Jerald, J., Kanagaraj, G., 2018. Effects of electrode materials on performance measures of electrical discharge micro-machining. Mater. Manuf. Process. 33 (6), 606–615.
Plaza, S., Sanchez, J.A., Perez, E., Gil, R., Izquierdo, B., Ortega, N., Pombo, I., 2014. Experimental study on micro EDM-drilling of Ti6Al4V using helical electrode. Precis. Eng. 38 (4), 821–827.
Pradhan, B.B., Masanta, M., Sarkar, B.R., Bhattacharyya, B., 2008. Investigation of electro-discharge micro-machining of titanium super alloy. Int. J. Adv. Manuf. Technol. 41 (11), 1094.
Pramanik, A., 2014a. Developments in the non-traditional machining of particle reinforced metal matrix composites. Int. J. Mach. Tool Manufact. 86, 44–61.
Pramanik, A., 2014b. Problems and solutions in machining of titanium alloys. Int. J. Adv. Manuf. Technol. 70 (5-8), 919–928.
Pramanik, A., Basak, A., 2016. Degradation of wire electrode during electrical discharge machining of metal matrix composites. Wear 346, 124–131.
Pramanik, A., Basak, A., 2018. Sustainability in wire electrical discharge machining of titanium alloy: understanding wire rupture. J. Clean. Prod. 198, 472–479.
Pramanik, A., Basak, A., Dixit, A., Chattopadhyaya, S., 2018a. Processing of duplex stainless steel by WEDM. Mater. Manuf. Process. 1–9.
Pramanik, A., Basak, A., Islam, M.N., Littlefair, G., 2015. Electrical discharge machining of 6061 aluminium alloy. Trans. Nonferrous Metals Soc. China 25 (9), 2866–2874.
Pramanik, A., Basak, A.K., Prakash, C., 2019. Understanding the wire electrical discharge machining of Ti6Al4V alloy. Heliyon 5 (4), e01473.
Pramanik, A., Islam, M.N., Boswell, B., Basak, A.K., Dong, Y., Littlefair, G., 2018b. Accuracy and finish during wire electric discharge machining of metal matrix composites for different reinforcement size and machining conditions. Proc. IME B J. Eng. Manufact. 232 (6), 1068–1078.
Pramanik, A., Littlefair, G., 2014. Developments in machining of stacked materials made of CFRP and titanium/aluminum alloys. Mach. Sci. Technol. 18 (4), 485–508.
Pramanik, A., Littlefair, G., 2015. Machining of titanium alloy (Ti-6Al-4V)—theory to application. Mach. Sci. Technol. 19 (1), 1–49.
Pramanik, A., Littlefair, G., 2016. Wire EDM mechanism of MMCs with the variation of reinforced particle size. Mater. Manuf. Process. 31 (13), 1700–1708.
Pramanik, A., Neo, K., Rahman, M., Li, X., Sawa, M., Maeda, Y., 2009. Ultraprecision turning of electroless nickel: effects of crystal orientation and origin of diamond tools. Int. J. Adv. Manuf. Technol. 43 (7-8), 681.
Prohaszka, J., Mamalis, A., Vaxevanidis, N., 1997. The effect of electrode material on machinability in wire electro-discharge machining. J. Mater. Process. Technol. 69 (1-3), 233–237.
Rao, P.S., Ramji, K., Satyanarayana, B., 2010. Prediction of material removal rate for aluminum BIS-24345 alloy in wire-cut EDM. Int. J. Eng. Sci. Technol. 2 (12), 7729–7739.
Sales, W., Oliveira, A., Raslan, A., 2016. Titanium perovskite (CaTiO3) formation in Ti6Al4V alloy using the electrical discharge machining process for biomedical applications. Surf. Coating. Technol. 307, 1011–1015.
Sarkar, S., Mitra, S., Bhattacharyya, B., 2005. Parametric analysis and optimization of wire electrical discharge machining of γ-titanium aluminide alloy. J. Mater. Process. Technol. 159 (3), 286–294.
Shabgard, M., Alenabi, H., 2015. Ultrasonic assisted electrical discharge machining of Ti–6Al–4V alloy. Mater. Manuf. Process. 30 (8), 991–1000.
Shen, Y., Liu, Y., Zhang, Y., Tan, B., Ji, R., Cai, B., Zheng, C., 2014. Determining the energy distribution during electric discharge machining of Ti–6Al–4V. Int. J. Adv. Manuf. Technol. 70 (1-4), 11–17.
Singh, P., Yadava, V., Narayan, A., 2018. Parametric study of ultrasonic-assisted hole sinking micro-EDM of titanium alloy. Int. J. Adv. Manuf. Technol. 94 (5-8), 2551–2562.
Sivakumar, K., Gandhinathan, R., 2013. Establishing optimum process parameters for machining titanium alloys (Ti6Al4V) in spark electric discharge machining. Int. J. Eng. Adv. Technol. 2, 201–204.
Sivaprakasam, P., Hariharan, P., Gowri, S., 2014. Modeling and analysis of micro-WEDM process of titanium alloy (Ti–6Al–4V) using response surface approach. Engineering Science and Technology, an International Journal 17 (4), 227–235.
Soni, J., 1994. Microanalysis of debris formed during rotary EDM of titanium alloy (Ti 6A1 4V) and die steel (T 215 Cr12). Wear 177 (1), 71–79.
Soni, J., Chakraverti, G., 1994. Machining characteristics of titanium with rotary electro-discharge machining. Wear 171 (1-2), 51–58.
Tang, J.J., Yang, X.D., 2018. Simulation investigation of thermal phase transformation and residual stress in single pulse EDM of Ti-6Al-4V. J. Phys. D Appl. Phys. 51 (13).
Tang, L., Du, Y., 2014. Experimental study on green electrical discharge machining in tap water of Ti–6Al–4V and parameters optimization. Int. J. Adv. Manuf. Technol. 70 (1-4), 469–475.
Tiwary, A., Pradhan, B., Bhattacharyya, B., 2015. Study on the influence of micro-EDM process parameters during machining of Ti–6Al–4V superalloy. Int. J. Adv. Manuf. Technol. 76 (1-4), 151–160.
Tsai, M., Fang, C., Yen, M., 2018. Vibration-assisted electrical discharge machining of grooves in a titanium alloy (Ti-6A-4V). Int. J. Adv. Manuf. Technol. 97 (1-4), 297–304.
Verma, V., Sajeevan, R., 2015. Multi process parameter optimization of diesinking EDM on titanium alloy (Ti6Al4 V) using Taguchi approach. Mater. Today: Proceedings 2 (4-5), 2581–2587.
Wansheng, Z., Zhenlong, W., Shichun, D., Guanxin, C., Hongyu, W., 2002. Ultrasonic and electric discharge machining to deep and small hole on titanium alloy. J. Mater. Process. Technol. 120 (1-3), 101–106.
Wasif, M., Iqbal, S.A., Fatima, A., Yaqoob, S., Tufail, M., 2020. Experimental investigation for the effects of wire EDM process parameters over the tapered cross-sectional workpieces of titanium alloys (Ti6Al-4V). Mech. Sci. 11 (1), 221–232.
Xie, B.-c., Wang, Y.-k., Wang, Z.-l., Zhao, W.-s., 2011. Numerical simulation of titanium alloy machining in electric discharge machining process. Trans. Nonferrous Metals Soc. China 21, s434–s439.
Yadav, U.S., Yadava, V., 2015. Experimental investigation on electrical discharge drilling of Ti-6Al-4V alloy. Mach. Sci. Technol. 19 (4), 515–535.
Yan, M.-T., Lai, Y.-P., 2007. Surface quality improvement of wire-EDM using a fine-finish power supply. Int. J. Mach. Tool Manufact. 47 (11), 1686–1694.
Yilmaz, O., Okka, M.A., 2010. Effect of single and multi-channel electrodes application on EDM fast hole drilling performance. Int. J. Adv. Manuf. Technol. 51 (1-4), 185–194.
Yunpeng, Z., Guangbiao, S., Anzhou, Z., 2014. Effect of mixed powder ultrasonic vibration on surface structure and mechanical properties of Ti-6Al-4V in Electro-Discharge Machining. Rare Met. Mater. Eng. 43 (1), 189–193.
Zhang, S.F., Zhang, W.C., Liu, Y., Ma, F.J., Su, C., Sha, Z.H., 2017. Study on the gap flow simulation in EDM small hole machining with Ti alloy. Adv. Mat. Sci. Engin. 2017, 8408793, 2017.
Zhang, Y.P., Sun, G.B., Zhang, A.Z., 2012. Study on the surface quality of titanium alloy in ultrasonic-assisted EDM milling. In: Paper Presented at the Applied Mechanics and Materials.